Hindawi
Advances in Civil Engineering
Volume 2020, Article ID 8493495, 24 pages
https://doi.org/10.1155/2020/8493495

Research Article

Seismic Performance Evaluation of RC Frame Designed Using Ethiopian and Chinese Seismic Codes

Kabtamu Getachew, Deng-Hong Chen, and Gang Peng

College of Civil Engineering and Architecture, China Three Gorges University, Yichang 443002, China

Correspondence should be addressed to Deng-Hong Chen; d.chen@ctgu.edu.cn

Received 15 September 2019; Revised 15 November 2019; Accepted 17 December 2019; Published 25 March 2020

Academic Editor: Andreas Lampropoulos

This study presents the seismic performance evaluation of the reinforced concrete (RC) frame designed as per Ethiopian (based on EN1998-1) and Chinese seismic codes to realize best practices within them. In the study, three-model RC frames with 4-, 8-, and 12-story are designed with the respective codes. Then, their seismic performances are evaluated using the nonlinear static (pushover) procedures of FEMA 356 and ATC 40 provisions. To validate the analysis result, dynamic nonlinear time history analysis is also made. The comparison parameters include elastic stiffness, peak strength, target displacement, and plastic hinge formation patterns in the structures. The results display many similarities in the global and local performances of the structures. Despite these, some noteworthy discrepancies are also noted. Besides, the performance point analysis revealed a significant difference in target displacement that reflects the two codes' demand spectrum essential disagreements, particularly for the period of vibration greater than 2.0's. In conclusion, the study highlighted the beneficial aspects of both codes, which will be useful for the future studies.

1. Introduction

Regardless of their differences, modern seismic building design codes tend to agree on issues of design methodology and the state-of-the-art in using different design control parameters such as a design base shear, capacity and demand ductility, and drift limits to ensure seismic performance [1]. Recently, many of the seismic codes have adopted performance-based seismic design in their updated seismic provisions. This overcomes the limitations of force-based design methods [2]. Moreover, the method is becoming attractive in the realization that increasing strength may not improve safety nor necessarily reduce damage [3]. It implies that structures and facilities can be designed and constructed in such a manner that their performance under expected seismic load can be estimated with an acceptable degree of accuracy [4], for commonly known three performance levels: serviceability (damage control), life safety, and collapse prevention [5]. To evaluate the performance levels, various seismic codes adopted either static or dynamic nonlinear analysis. So far, many of them adopted FEMA 356 [6] and ATC 40 [7] standards as benchmarks in their seismic performance evaluations. Yet, the codes with their particular provisions still apply linear elastic analysis for force-based design; if employed for a given structure, the seismic performance of the structure will be dissimilar, either desirable or not. Consequently, various codes' seismic performance comparisons are becoming popular nowadays worldwide for learning from one another in the design of seismic buildings for optimized design and verification [1, 8–10]. Hence, comparing different seismic codes enables the enrichment of beneficial aspects obtained within them. Bearing this in mind, this study compares Ethiopian and Chinese codes for the reasons presented in the following sections.

Firstly, a building code adoption from one country to another is a common practice. Particularly, the rapid urbanization in developing countries, such as African countries, demands international contractors with better financial capacity and technical skills. For example, Chinese international contractors are constructing 12 to 40 more

multistory building projects in Addis Ababa, the capital of Ethiopia in East Africa [11–13]. Such projects may use the Chinese construction standards as they already experienced in their country construction [14], despite the local code being different. However, compared with Ethiopia, China is one of the high seismic countries in the world and has developed its own seismic code GB50011-2010 (GB11-10, hereafter) [15], which is the outcome of several updates since 1959 [16]. In contrast, Ethiopia, an East African country, is an earthquake sensitive region, though the magnitude is less than other countries on other continents. The rift valley passes through the central part of Ethiopia where major Earthquakes and volcano do occur [17, 18]. At the same time, economically more important cities are emerging rapidly recently in this region [17]. This will be very devastating for developing countries like Ethiopia, with little preparation for an earthquake as noted in Haiti [19]. Yet, Ethiopia did not develop its seismic code so far, and it has been adopted from Western developed countries [18]. Likewise, the current seismic code of Ethiopia (2015) named Ethiopian Standard for seismic design ES8-2015 (ES8-15, hereafter) and other related structural codes are also based on European Norms EN1998-1 [20] similar to Eurocode 8-2004. Accordingly, throughout this study, ES8-15 follows Eurocode 8-2004 provisions and its related past studies to compare with Chinese code GB11-10.

Secondly, Eurocodes are also claimed to be the most technically advanced structural codes in the world and are proposed to provide worldwide access to designers and mostly adopted in countries that having historical relations with UK [21]. At the same time, the Chinese companies working on international projects also use them as a reference [22].

Thirdly, although many improvements are made in the latest Chinese seismic code GB11-10 [15] and Technical Specification for Concrete Structures of Tall Building JGJ3-2010 [23], none of the tall buildings in China have experienced a truly strong earthquake so far and the study of other countries' codes with advanced seismic design philosophies is relevant [24]. USA and China seismic code comparison results indicate that the seismic design forces determined by the Chinese response spectrum are larger than those determined by the US design spectrum, though the seismic performance is nearly the same [25]. The performance assessment of a 5-story RC frame designed by GB11-10 satisfies the performance limits as per ASCE/SEI 41-06 and also highlighted some weaknesses to be improved [26]. The comparative study of seismic provisions for the design of steel moment frames showed the conservativeness of the Chinese code over Eurocode-8 [9]. Moreover, in our recent work, soil structure interaction, dynamic analysis of RC frame subjected to the same ground motion matched to the design response spectrum of ES8-15 and GB11-10, higher base shear, and interstory drift observed in GB11-10 [27].

To this end, the comparison between the Chinese and Ethiopia code is very relevant. As noted above, little work was done on the seismic performance assessment of RC frame designed with the respective codes as compared with the efforts made on the steel frame. To the authors' knowledge, only research done by Li et al. [28] attempted to compare Eurocode 8-2004 with old Chinese Seismic Code GB50011-2001 [29] for a 6-story RC frame design. Other related comparisons are not complete, either in the response spectrum or the base shear comparison alone, which may give misleading results as noted in [1]. Hence, the study presents the design and seismic performance assessment of selected model frames according to Ethiopian and Chinese seismic codes in the subsequent sections based on building structures critical seismic performance evaluation parameters such as plastic hinges formation, capacity curve, interstory drift, and target displacement.

2. Methods of the Study

For this study, a group of regular two-dimensional (2D) reinforced concrete (RC) moment-resisting frames composed of 4-, 8-, and 12-story residential buildings are designed according to the specifications outlined in Ethiopian and Chinese seismic codes with capacity design principle. All the models are designed for similar conditions of loading and design material strength by avoiding geographic location differences. Subsequently, the seismic performance analysis is made using a nonlinear static (pushover) method as per FEMA 356 and ATC 40 provisions. A pushover-based analysis represents a rational practice-oriented tool for the seismic analysis of structures. Compared with traditional elastic analyses, it provides a wealth of additional important information about the expected structural response, as well as insight into the structural aspects that controls performance during severe earthquakes. Furthermore, it exposes design weaknesses that could remain hidden in an elastic analysis; for example, in most cases, it can detect the most critical parts of a structure, despite its limitations [30]. It is preferred as the considered model buildings are regular and first mode dominant [31]. Moreover, for verification of nonlinear static analysis, nonlinear dynamic analysis is also made.

3. Analytical Model of Reinforced Concrete Frame

This section provides a brief design procedure of the model buildings considered in the study using both codes, here the Ethiopian and Chinese building codes. Subsequently, the design results will be used as an input for seismic performance assessment of the models in Section 4. To examine the design methods and seismic provisions in the two codes, the material strength, loading, and geometric models were kept nearly similar.

3.1. Geometric Model, Material Strength, and Gravity Load. For the analytic model of buildings in this study, we adopted a structural plan from our previous work as shown in Figure 1(a), residential building with a plan layout of $15\,\text{m} \times 32\,\text{m}$ with central model frames in the transverse direction [27]. In the models, we have two types of reference

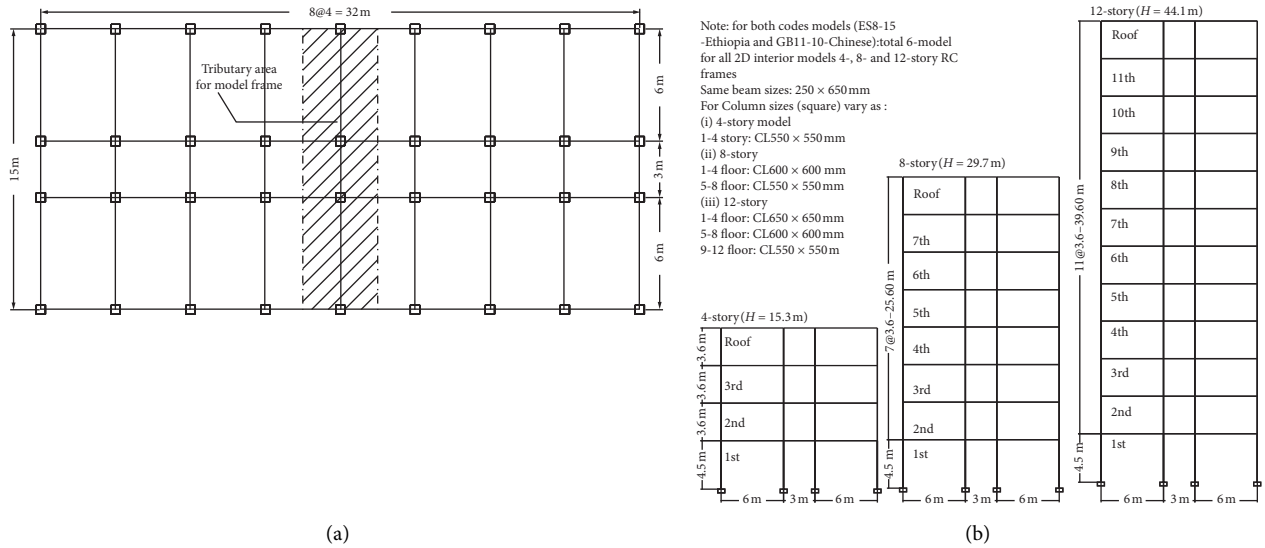

Figure 1: (a) Typical floor plan of A and B model building [27] and (b) 4-, 8-, and 12-story model frames of A and B.

frames, A and B, which are designed according to ES8-15 (EN1998-1) and GB11-10 respectively. Figure 1(b) shows each model has a pair of three typical frames totally six model frames with all fixed bases. The two codes' model frames are assigned the same beam and column dimension as indicated in Figure 1(b). It also shows the column sections vary in 8- and 12-story frames, while the beam section is kept similar in all floor levels. The story height of the ground floors was 4.5 m, while the height of the remaining typical stories was 3.6 m.

For the design of beam and column cross-sections, nearly the same concrete and reinforcing steel strengths are considered as per corresponding concrete codes of Chinese GB50010-2010 [32] and Ethiopian ES2-2015 [33]. Concrete compressive strength at 28 days (C-30/C-25/30), elastic modulus of concrete, $E_C = 31 \times 10^6\,\text{kN/m}^2$, concrete unit weight = 25 kN/m^3, reinforcement steel strength = steel S-400/HRB400, $E_s = 200 \times 10^6\,\text{kN/m}^2$, and steel unit weight = 78.5 kN/m^3. The stress-strain of concrete in both ES2-2015 (European) and Chinese GB50010-2010 follows the same H. Rusch formula [34] for designing members.

The design load includes both gravity and seismic lateral load. Gravity load comprises the dead load, including the self-weight of the structure and live load applied on the floor. The dead load, including slab self-weight, was set as 6.0 kN/m^2. Besides the dead load of the infill walls, the distributed load on the typical beams is set to 10 kN/m. In addition, both codes consider the same live load of 2.0 kN/m^2 according to ES1-2015 [35] and GB50009-2012 [36]. Finally, the floor loads are transferred to floor beams of the model frames. Besides this, for the dynamic analysis of the frames, the codes consider 30% and 50% of the live load in ES8-15 and GB11-10, respectively, in addition to dead load, for seismic mass calculation.

3.2. Design Seismic Input: Design Response Spectrum. For the seismic design, the two codes consider different seismic design hazard levels of ground motion in their design response spectrum. The Ethiopian Seismic Code ES8-15 [20] specifies two levels of ground motion. In the first case, the reference ground motion is associated with a probability of exceedance equal to 10% in 50 years, a return period of 475 years. For this level, no local or global collapse of a structure is permitted (i.e., no-collapse requirement, which refers to the ultimate limit state). The other one has a probability of exceedance equal to 10% in 10 years or a return period of 95 years and structures are designed to have sufficient resistance and stiffness to maintain the function of vital services, without the occurrence of damage, and the associated limitations in use refer to damage limit. The reference peak ground acceleration, PGA (a_{gR}) map, is used to classify Ethiopia seismicity mainly into five (5) seismic zones 1 (0.04 g), 2 (0.07 g), 3 (0.10 g), 4 (0.15 g), and 5 (0.20 g) for noncollapse requirement. The damage limitation 0.40 to 0.50 times that of the noncollapse requirement.

On the other hand, the Chinese seismic code GB11-10 [15] defines three-level seismic performance requirements, which essentially refer to serviceability (operational), damageability (damage-repairable), and survivability (collapse-prevention) limit states, respectively. The operational and collapse-prevention requirement corresponds to ground motion based on a recommended probability of exceedance of 63% and 2%-3% in 50 years, a return period of 50 and 1600–2400 years, respectively, while the values associated with the damage-repairable level relate to a recommended probability of exceedance of 10% in 50 years, a return period of 475 years. In the Chinese code, different regions are categorized by the Mercalli intensity scale to describe the effects of seismic action on structures. Seismic active regions are categorized into 4 groups with an intensity of 6, 7, 8, and 9, respectively [15, 37]. The reference peak ground acceleration (PGA) is defined with a 10% exceedance in 50 years (Table 11 in Appendix-A), which corresponds to the four intensity groups, 6 (<0.1 g), 7 (0.10/0.15 g), 8 (0.20/0.3 g), and 9 (0.40 g). For this study, the 10% exceedance in 50 years commonly available in both codes is considered.

Based on the seismic design hazard level, the codes define their response spectrum, which contains various parameters. The typical smooth codes response spectrum curves defined by Se (T) of Ethiopian and Chinese Seismic influence the coefficient curve (α) versus the period of vibration (T), respectively, is given in Appendix A. For more detail, the codes' response spectrum curve ordinates equations are presented in Figure 16 in Appendix A (a) ES8-15 and (b) GB11-10. ES8-15 response spectrum defined Se (T) based on a single-parameter PGA (peak ground acceleration) of two types of response spectrum with Type 1 (used in this study) strong intensity ($M > 5.5$) and Type 2 small intensity ($M < 5.5$). The response spectrum is defined with corner periods T_B, T_C, and T_D defined up to $T = 4.0$ s for various soil types. For the Chinese Code, the response spectrum ordinate α (T, T_g, α_{max}) is given as a fraction of the acceleration of gravity, where T is the natural vibration period of a building and T_g is the soil characteristic period at which the constant velocity branch starts in the response spectrum curve (Appendix A), which depends on the near or far source (design group) and soil class. α_{max}, maximum seismic influence coefficient, is given for the three levels of seismic hazard (Table 11 in Appendix A) and with respective seismic region categories [23]. The response spectrum of the codes depends on the soil type (ground type) to define corner periods and soil amplification factors. Shear velocity (V_{30}) is the common criterion used to classify soil in the two codes. The Chinese code GB11-10 has four soil classes from I to IV [15]. Whereas, the Ethiopian code ES8-15 classifies ground into five main groups A to E to account for the influence of local ground conditions on the seismic action with their respective soil amplification factor (S), while S-factor is not explicitly available in GB11-10.

Hence, based on shear velocity, the ground-type equivalency between the two seismic codes is required. For our study, we selected soil II (GB11-10, V_{30}, 280 m/s to 500 m/s) equivalent to soil B (ES8-15, V_{30} 360 m/s to 800 m/s). Note that, the Chinese PGA is measured with reference to stiff ground, soil II [32, 35, 41], while in Ethiopia, PGA is measured with reference to rock ground type A [17, 20].

According to [38] for a given city in China, the parameters of ground motion peak ground acceleration (PGA) in terms Ethiopian code ES8-15(EN1998-1) can be converted using equation (1a), and for a certain city in Ethiopia, the corresponding design ground motion parameters of the Chinese code GB11-10 can be determined by equation (1b) [9, 38]:

$$a_{g\mathrm{ET}(A)} = \frac{a_{g\mathrm{CH}}}{S}, \tag{1a}$$

$$a_{g\mathrm{CH}} = a_{g\mathrm{ET}(A)}\mathrm{S}, \tag{1b}$$

where agET (A)is the PGA of Ethiopia in terms of soil type A, S is the soil amplification factor, type 1 response spectrum, $S = 1.2$ (Soil B), and agCH is the PGA of China in terms of soil II, equivalence reference to soil B in Ethiopia. In this paper, China's city is taken as a reference and PGA is taken reference to soil type II and equation (1a) will be used throughout the study. For this study, the equivalent stiff soils with seismic intensity-7 (0.15 g measured reference to soil II) in GB11-10 and equivalently 0.125 g (ground Type A) in ES8-15 is used in model building design in Section 3.3.

Furthermore, the two codes practice the response spectrum in different ways to determine the design seismic input load to the model buildings. The Ethiopian code ES8-15 adopts the design response spectrum (also called the inelastic response spectrum) in addition to the elastic one (Appendix A). It is obtained by modifying the elastic spectrum by ductility and behavior factor, q, of a structure for elastic (linear) analysis, accounting for nonlinear effect used in the design of structural member sections. The behavior factor q is the capacity of structural systems to resist seismic actions in the nonlinear range. It is an approximate ratio of the seismic forces which the structure would experience if its response was completely elastic with 5% viscous damping to the seismic forces. It may be used in the design, with a conventional elastic analysis model, ensuring a satisfactory response of a structure. The value of the behavior factor, q, depends on the structural system. For RC building, the value of q is with the range of 1.5 to 6.75 as per [20], the value varies with ductility of the design and regularity of the structure, and the exact value needs nonlinear analysis. On the other hand, such a factor is not explicitly available in GB11-10; instead, frequent earthquake seismic action intensity level is adopted for elastic analysis and structural member design, which is a nearly constant value of 1/3 of the moderate earthquake (Table 11 in Appendix A).

Figure 2 compares the two codes' response spectrums. The graph is drawn, for the same seismic hazard design of level 10% exceedance in 50 years, with 5% damping, GB11-10 (PGA = 0.15 g, which is measured with reference to the ground type II seismic intensity 7), and equivalent to soil B with a soil amplification factor of $S = 1.2$ in ES8-15 (PGA = 0.125 g, measured with reference to ground type A). The elastic response spectrum comparison shows good similarity for a period of vibration $T < 2.0$ s. Yet, GB11-10 is significantly greater than ES8-15 by 1.85 to 3.0 times for a long period of vibration $T > 2.0$ s. Such differences in the elastic spectrum will affect the performance point analysis (shown in Section 5.4) and nonlinear dynamic analysis (when the elastic spectrum is used as a target spectrum for matching various ground motions).

Besides, Figure 2 also displays the design (inelastic) response spectra of ES8-15 with a behavior factor $q = 5.85$ (ductility high RC frame) and GB11-10 with frequent earthquake (63% in 50 years) design level. For a shorter period, clearly, GB11-10 gives a larger response. Nevertheless, in a longer period of vibration $T > 2.0$ s, the minimum values of both response spectra are nearly the same, unlike the elastic response spectra of ES8-15. One can note that the seismic demand in 10% in 50 years is reduced to design value nearly by 1/3 and 1/5.85 in GB11-10 and ES8-15, respectively. These spectrums are applied at the base of the model frames together with the gravity loads and performing linear analysis for structural members' design.

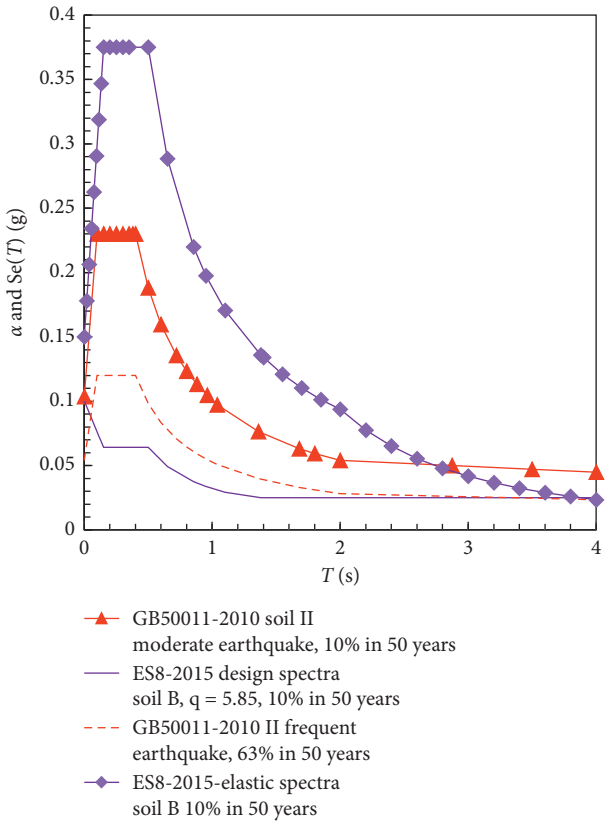

Figure 2: Design response spectrum of GB11-10 and ES8-15.

3.3. Structural Analysis and Design. The model frames' structural analysis and design was performed with the aid of the Software Midas Gen [39], which incorporates both ES8-15 (Eurocode 8-2004) and Chinese code (GB11-10). In the analysis of all models, gross beam and column stiffness are considered. Modal response spectrum analysis (RSA) is performed for the ground excitation in horizontal directions. Figure 2 shows the codes' design spectrum considered for horizontal directions. The complete quadratic (CQC) rule for the combination of different modes responses was used as per ES8-15 and GB11-10 recommendation. Figure 3 and Table 1 present the modal analysis results of the model frame. Figure 3 shows the modal shape of the first three modes shapes displaying little differences between parallel modes as the members' cross section similar except live load consideration difference. Besides, Table 1 displays the first three modal properties of the building with modal mass participation factor and natural periods. For all models (A-ES8-15) and (B-GB11-10), the first modal mass participation factors are nearly 80% or more, displaying a first-mode dominant structure.

3.4. Design of Structural Members. The columns and beams of frames A and B are designed using the concrete codes of Ethiopia, ES2-2015 [33], and China, GB50010-2010 [32], considering the respective seismic provisions. The horizontal seismic action and gravity load were considered as the main load applied to the reference structure. The design value of the load effect in the structural components is determined using a ductile capacity design method to avoid brittle failure. GB11-10 recommends different special seismic provision grades for seismic design based on seismic intensity, structural type, and height (H) of structure. In this study of the framed structures subjected to seismic intensity of 7, PGA = 0.15 g, for both 12-story ($H = 44.1$ m) and 8-story, $H = 29.70\,\text{m} > 24.0\,\text{m}$ Grade-2, whereas for 4-story, $H = 15.30 < 24.0$ m, and for Grade-3, the seismic design adopted. On the other hand, the ES8-15 designs are for high-ductility RC frames, design provisions with a behavior factor, $q = 5.85$. Applying the principle of the capacity design method, the ductile design is made by using the corresponding seismic code provisions available in Midas Gen software [39]. From capacity design, the minimum joint strong column-weak beam ratio is 1.89 and 1.28 in 4-story, 2.36 and 1.32 in 8-story, and 2.39 and 1.21 in 12-story in seismic codes of ES8-15 and GB11-10, respectively. Figure 4 shows the 8-story typical design detailed drawings together with Table 2, for 4 and 12 stories (Appendix B), showing that the design result from both seismic standards has similarities and differences. Table 3 displays ES8-15 assigns more reinforcement in columns as compared with GB11-10, while for the beams, the reverse is noted. Nevertheless, the total amount reinforcement for each model frames is nearly equal in both codes.

4. Seismic Performance Assessment

4.1. Nonlinear Static Analysis. Nonlinear static (commonly known as pushover) analysis is a specialized procedure used in performance-based design for seismic loading [40]. For this study, SAP2000 Version 14.0.0 [41] computer program is used for pushover analysis of the model frames with 4-, 8-, and 12 stories designed in Section 3. In the pushover analysis, the two most important steps are defining plastic hinge properties and lateral load pattern, which entirely affect the analysis outcome at the global and member levels. For the analysis in SAP2000, the lumped plastic hinge properties are used. Figure 5 shows a typical force-deformation relationship behavior of a plastic hinge defined by FEMA-356 [6] with the required acceptance criteria of immediate occupancy (IO), life safety (LS), collapse prevention (CP), and collapse (C). In Figure 5, point A corresponds to the unloaded condition of the hinge deformation. Point B represents the yielding of structural elements that are controlled by moment-curvature relationships. Hinge deformation shows the strength degradation at point D, where the structure might show sudden failure after this point. The failure of the structure can be defined by reaching the points D and E. In addition, FEMA 356 [6] default hinges in SAP2000 are based on the earthquake code of the United States code.

However, the user-defined hinge model is better than the default-hinge model in reflecting the nonlinear behavior compatible with the element properties, which affects the seismic performance [42, 43]. In addition, the model members are designed using Ethiopian and Chinese code.

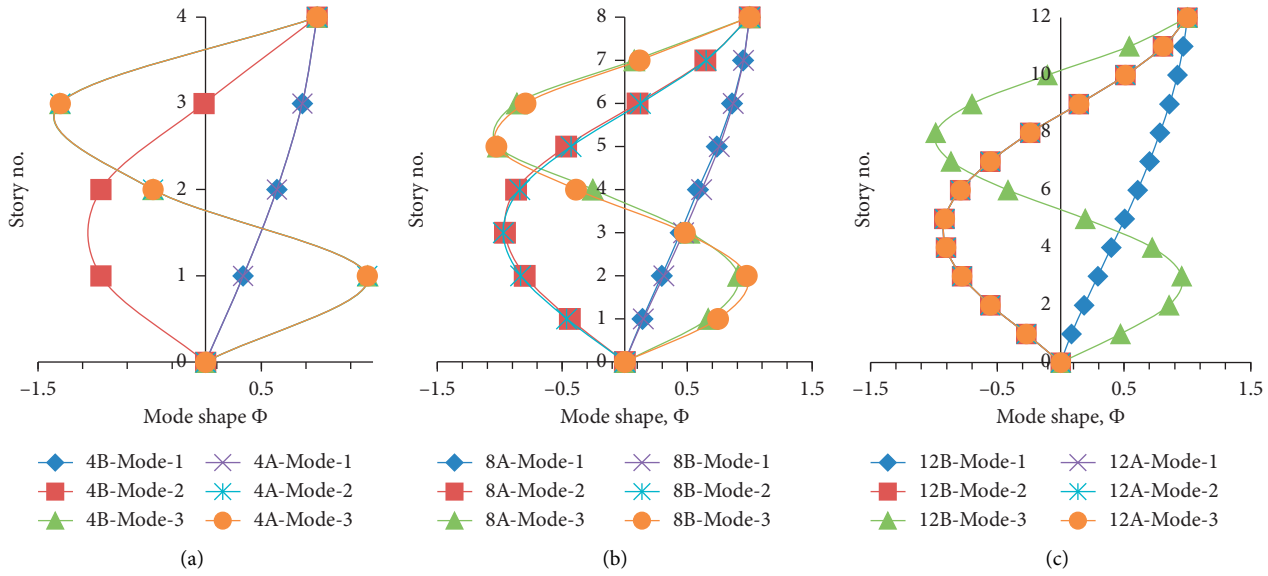

Figure 3: Modal shapes: (a) 4-(A, B), (b) 8-(A, B), and (c) 12-(A, B) story model frames.

Table 1: Seismic masses, natural periods, and modal participating mass (MPM (%)).

Structures	Mass (tonnes)	Modal characteristics						Sum of MPM (%)
		First mode		Second mode		Third mode		
		T_1 (s)	MPM%	T_2 (s)	MPM%	T_3 (s)	MPM (%)	
4A	306.49	0.60	88.72	0.19	8.86	0.10	2.04	99.62
8A	622.42	1.13	82.70	0.37	10.86	0.100	3.39	96.95
12A	960.32	1.66	79.75	0.55	11.44	0.205	3.91	95.10
4B	313.69	0.63	88.72	0.20	8.86	0.311	2.04	99.62
8B	642.23	1.17	82.64	0.38	10.90	0.22	3.41	96.94
12B	990.05	1.74	79.77	0.60	11.43	0.33	3.91	95.11

Hence, in this study, user-defined plastic hinge properties are adopted and calculated using the Xtract Software [44] from moment-curvature relations, for designed members in Section 3 (Table 2) based on confined concrete stress-strain [45] and reinforcement steel bilinear stress-strain curve for a similar design concrete grade C-30 and steel HRB400 (S-400), respectively, defined according to both concrete codes [32, 33]. For the moment-curvature analysis, the axial loads in the beams were assumed to be zero. While, for columns, axial loads were assumed constant and equal to the load due to the dead loads plus 30% and 50% of the live loads on the columns for ES8-15 and GB11-10, respectively. Besides, for columns, moment-axial force interaction diagram is also calculated. For the moment-rotation relationship as input in SAP2000, the plastic hinge length is used to calculate ultimate rotation values from the ultimate curvatures [42]. For each plastic hinge, plastic rotation $\theta_p = (\phi_u - \phi_y) * L_p$, where ϕ_y and ϕ_u are the yield and ultimate moment curvatures, respectively, where L_p is the plastic hinge length equal to 0.5 h, where h is the depth of a beam or column section is taken [46, 47]. Moreover, the three performance levels (Figure 5) are defined in terms of plastic rotation. IO, LS, and CP correspond to 20%, 50%, and 90% of the plastic-rotation capacity, respectively [6, 7]. Since all gravity loads are distributed uniformly on the beams, the potential plastic hinges are considered at both ends of the columns and beams. Similar to the FEMA 356 plastic hinges, in SAP 2000 column axial-moment hinge (P-M3), beam flexural moment hinges (M3) are defined at the end of the members. Then, the calculated nonlinear properties based on the sectional analysis are imported to each hinge. FEMA 356 recommends the flexural plastic hinges shall not be far away from component ends unless they are explicitly accounted for modeling and analysis [6]. Plasticity in RC members was assumed to be lumped at the probable location and was assumed to form at a distance equal to one-half of the average plastic hinge length L_p from the member ends as per [48].

Besides the plastic hinge, defining the lateral load pattern is another most important issue in pushover analysis. FEMA 356 [6] and ES8-15 [20] recommend the use of more than one lateral load pattern to bound the range of design actions that may occur during the actual dynamic response of a structure during an earthquake. In this study, we employ uniform and Mode-1 (nearly the same to triangular) load patterns. The uniform load pattern is based on lateral forces that are proportional to mass regardless of elevation (uniform) response acceleration. Another one, a modal pattern,

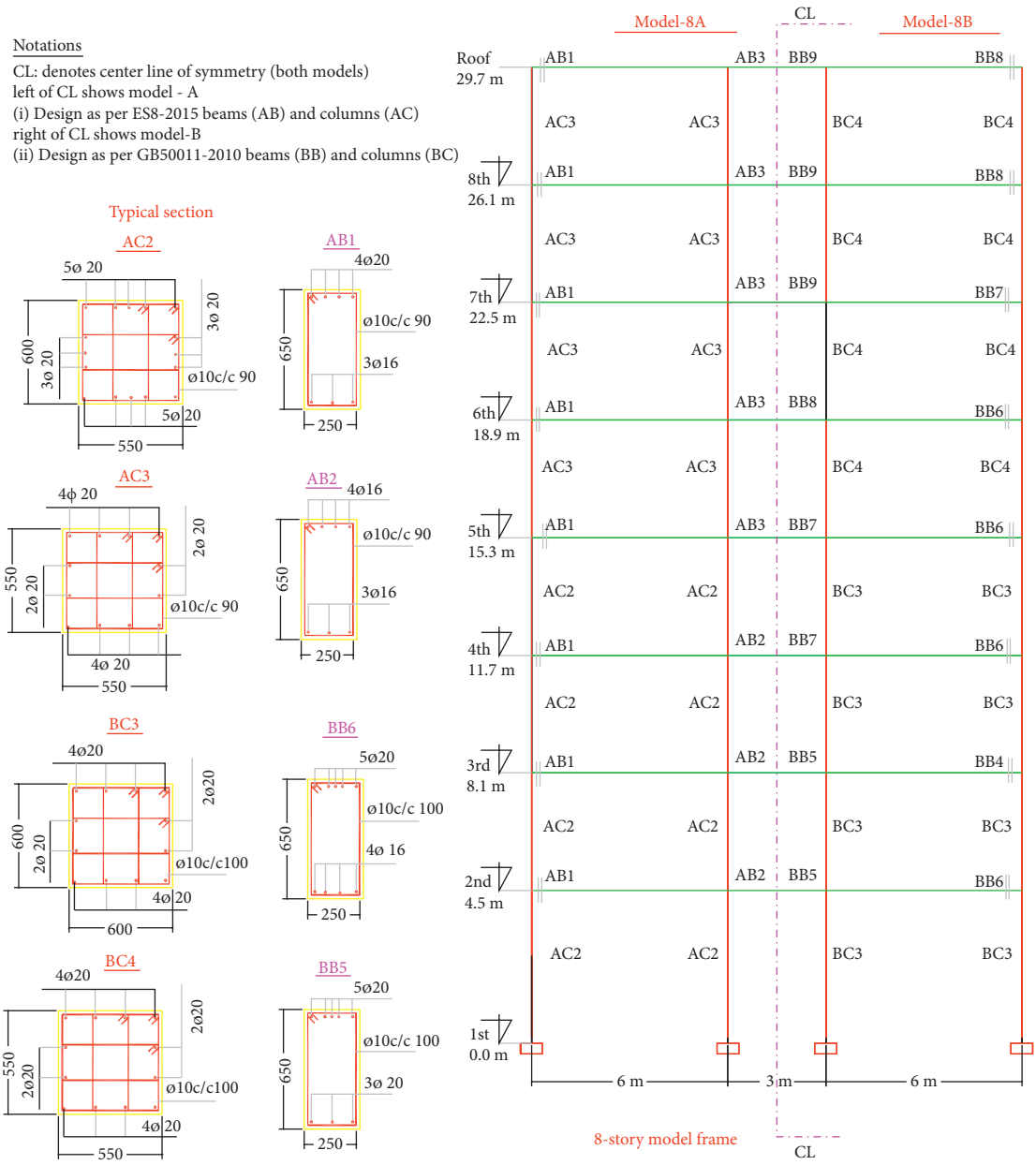

Figure 4: Reinforcement design diagram 8-story RC frame designed as per ES8-15(8A) and GB11-10 (8B).

Table 2: Beam and column section reinforcement design of 8-story frame in Figure 4.

Cross type	Building-8A ES8-15						Building-8B GB11-10		
	Cross section	Rebar top (T) bottom (B)	Stirrup (mm)	Cross section	Rebar top (T) bottom (B)	Stirrup (mm)	Cross section	Rebar top (T) bottom (B)	Stirrup (mm)
Beam	AB1-25 × 65	4Φ20(T) 3Φ16(B)	90	BB4-25 × 65	6Φ20(T) 4Φ16(B)	100	BB7-25 × 65	4Φ20(T) 4Φ16(B)	90
	AB2-25 × 65	4Φ16(T) 3Φ16(B)	90	BB5-25 × 65	5Φ20(T) 3Φ20(B)	100	BB8-25 × 65	3Φ20(T) 4Φ16(B)	90
	A B3-25 × 65	3Φ16(T) 3Φ16(B)	90	BB6-25 × 65	5Φ20(T) 4Φ16(B)	100	BB9-25 × 65	4Φ16(T) 4Φ16(B)	90
Column	AC2-60 × 60	16Φ20	40	BC3-60 × 60	12Φ20	100			
	AC3-55 × 55	12Φ20	90	BC4-55 × 55	12Φ20	100			

Table 3: Longitudinal rebar (kilogram) quantity in column and beam for model frame designed.

Model frame	ES8-15 (rebar)-A			GB11-10 (rebar)-B			B/A	B/A	B/A
	Beam	Column	Total	Beam	Column	Total	Beam	Column	Total
4-story	823.47	1,544.72	2,368.20	874.35	1,351.63	2,225.98	1.06	0.875	0.94
8-Story	1,642.21	4,117.37	5,759.58	2,040.64	3,513.96	5,554.60	1.24	0.853	0.96
12-Story	2,340.27	6,389.02	8,729.30	3,538.51	5,519.40	9,057.92	1.51	0.863	1.04

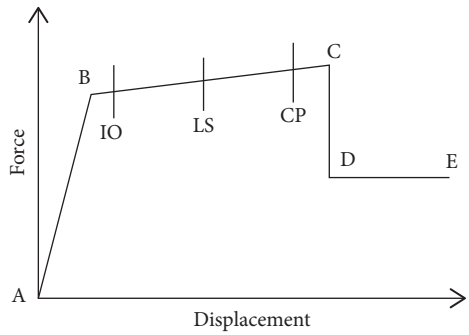

Figure 5: Force-deformation relationship of a plastic hinge [6, 40].

is proportional to lateral forces consistent with the lateral force distribution along the height of structure. The modal pattern, hereafter Mode-1, and lateral force pattern are obtained from the first mode shape of modal analysis and normalized so that the force at the top is equal to 1.0. With these load patterns, the pushover analysis is performed using SAP2000 software [41], which gives a pushover capacity curve that relates base shear (V) to roof displacement (Dt) relationship.

The pushover capacity curve shows the overall capacity of the structure for sequentially increasing control node displacement from zero to the target displacement. The control node displacement may be taken at the center of mass the roof of the model frames. The value of the roof displacement is the expected displacement during an earthquake in the nonelastic range. ES8-15 (EN1998-1) [20] and FEMA 356 [6] recommend 150% target displacement. Alternatively, it can be calculated from the target inelastic drift ratio, target rotational ductility, and height of the building [7, 49, 50]. ATC 40 recommends 2% roof drift; the deformation limit given for the life safety performance level appears to be a good stopping point for the pushover analysis. For this study, 2% H roof drift is considered for the control node displacement of all models, where H is the height of the building and hence the applied roof drift to each model will be 0.30 m ($H = 15.3$ m), 0.60 m ($H = 29.70$ m), and 0.88 m ($H = 44.10$ m), respectively, for 4 (A/B), 8 (A/B), and 12 (A/B) story frames. In the analysis, the displacement control method of pushover analysis is preferred since the amount of load is unknown and useful for structures that become unstable and may lose load-carrying capacity during the analysis [40]. Also, note that the P-delta effect is not included here.

4.2. Nonlinear Dynamic Analysis. In order to verify the results obtained by the nonlinear static pushover analysis (SPO, hereafter), dynamic nonlinear time-history analysis (NL-THA, hereafter) was conducted [51, 52]. It is widely recognized that the NL-THA is more accurate than SPO analysis, but choosing the appropriate ground motions is not a simple task. For a given specific building site, it involves various parameters as ground motions are not easily available everywhere. In the absence of such ground motion data for the considered building models, a set of seven natural acceleration records, selected within the most frequently used records, was considered from the PEER database [53]. The selected ground motions are with a shear velocity range of 360 to 500 m/s at the recording station to make it consistent for designed model frame bases, equivalent ground types, and soil B and II in Ethiopian and Chinese seismic codes, respectively. Table 4 shows the seven unscaled selected ground motions from various parts of the world. The selected recording stations have horizontal acceleration with a PGA value of 0.089 g to 0.75 g. Then, they are matched to elastic response spectrums of ES8-15 soil B (PGA = 0.25 g – soil class A) and GB11-10 soil II (PGA = 0.30 g – soil class II) using Seismomatch software [54]. The minimum and maximum matching periods of $0.2T_1$ and $2T_1$, respectively, are considered as per ES8-15 recommendation, where T_1 is the fundamental period of vibration of the considered model frame. Figure 6 shows the ground motion spectrums matched to the two codes spectrum for 8-story model frames. All the acceleration records were scaled to the same PGA value. Besides this, artificial acceleograms are generated for same PGA used in matching real accelegromas. Correspondingly, seven artificial time-history records were generated using SeismoArtif software [55] for peak ground acceleration of $0.3g$ and soil class B and II with a 5% viscous damping ratio. The earthquake duration was set to 30 s. The artificial accelerograms are used in evaluating the structural responses together with matched real accelerograms.

For the dynamic analysis, the basic modeling approaches and acceptance criteria of the NL-THA are identical to those for the SPO [6, 56]. Hence, the same model frames in SPO analysis are adopted to conduct NL-THA analysis in SAP2000 version 14.0.0 computer program [41]. The matched ground motion records are imported to the analysis model. For an illustrative purpose, only 8-story model frames are analyzed using NL-THA in both codes and results are compared with SPO results. For each matched real ground motion records, the dynamic analysis is made and repeated by scaling values of PGA ranging from 0.3 g to 1.20 g, which is also called incremental dynamic analysis [57], for plotting dynamic pushover capacity curve. Additionally, using artificial synthetic ground motions, NL-THA

Table 4: PEER ground motion data NGA West-2.

S no.	Earthquake name	Year	Recording station number (RSN)	Magnitude	Vs30 (m/sec)	Peak ground acceleration PGA (g)
1	Mammoth lakes-01, US	1980	230	6.06	382.12	0.42
2	Loma Prieta, US	1989	802	6.93	380.89	0.51
3	Chi-Chi_Taiwan	1999	1513	7.62	363.99	0.59
4	Northridge-01, US	1994	1004	6.69	380.06	0.75
5	Parkfield-02_CA, US	2004	4070	6.00	378.99	0.62
6	Landers, US	1992	832	7.28	382.93	0.089
7	Imperial valley-06, US	1979	164	6.53	471.53	0.21

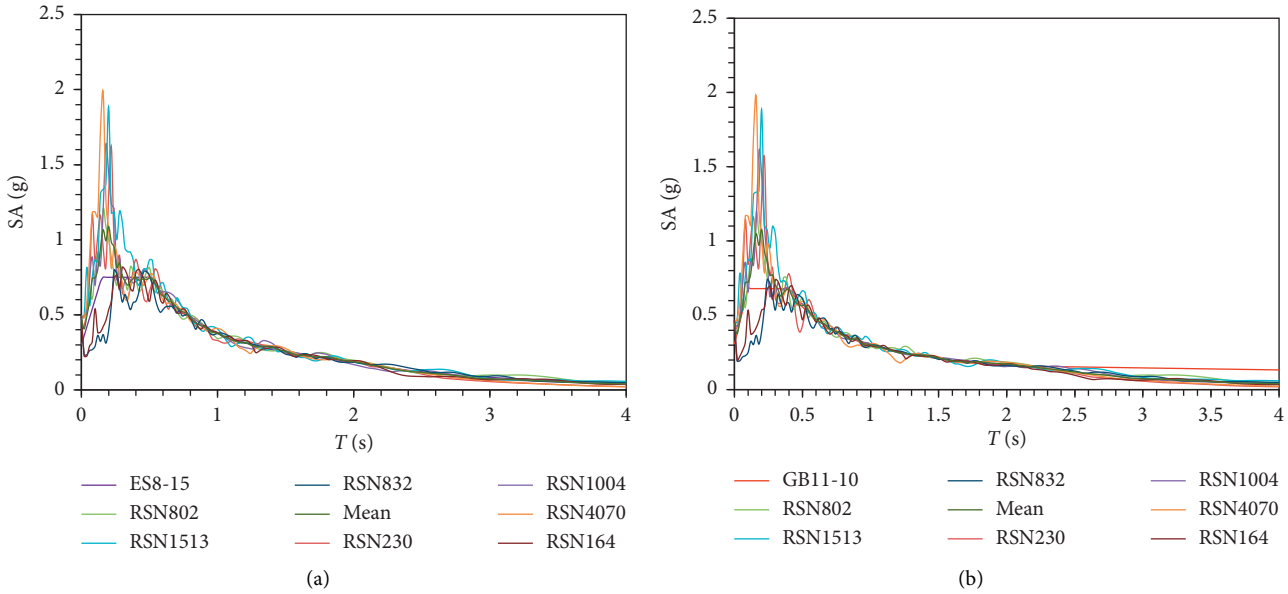

Figure 6: Matched response spectrum for (a) 8A and (b) 8B-Model Buildings (for PGA = 0.3 g, soil II, and 0.25 g, soil-A).

is made for scaled PGA values of 0.30 g and 0.6 g to compare structural responses such as plastic hinges and drifts with SPO results.

5. Results and Discussion

This section presents the performance assessment analysis results. Section 5.1 presents an illustrative example for the verification of the pushover analysis, using nonlinear time history (NL-THA) analysis. Sections 5.2–5.4 deal with the detailed discussions of the two codes' SPO analysis of model frames based on capacity (pushover) curves, interstory drift, pattern of plastic hinge formation, plastic hinges distribution in the structural elements, performance point assessment of each model based on the provisions and accepted criteria adopted in FEMA 356 [6], and ATC 40 [7] together with the respective code provision.

5.1. Verification of Nonlinear Static Analysis. This section presents an illustrative example of an 8-story model frame analysis made using both SPO and NL-THA, based on pushover capacity curve, roof drift, interstory drift, and plastic hinge formation. Figure 7 presents the static pushover and dynamic pushover capacity curves. The dynamic pushover curve was obtained for average 7 real ground

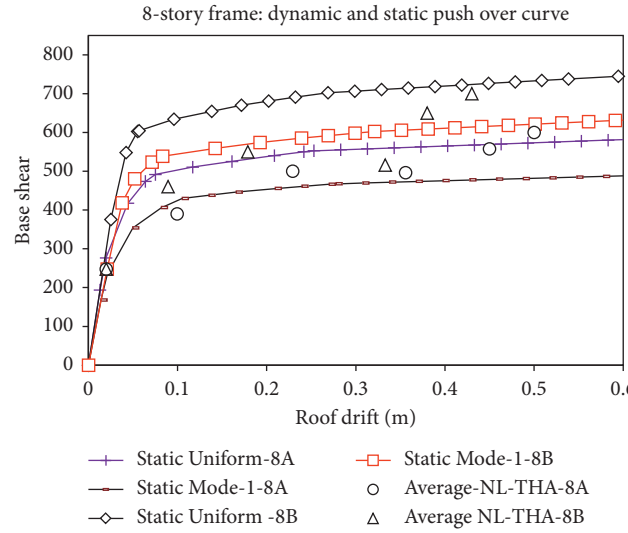

Figure 7: Static and dynamic pushover curve (a) 8A and (b) 8B Model frames.

motions closer to Mode-1 than uniform load pattern at the beginning of the curve, but it approaches uniform load pattern gradually. In both the static and dynamic capacity curves, the Model-8B (GB11-10) shows a bigger capacity than Model-8A (ES8-15).

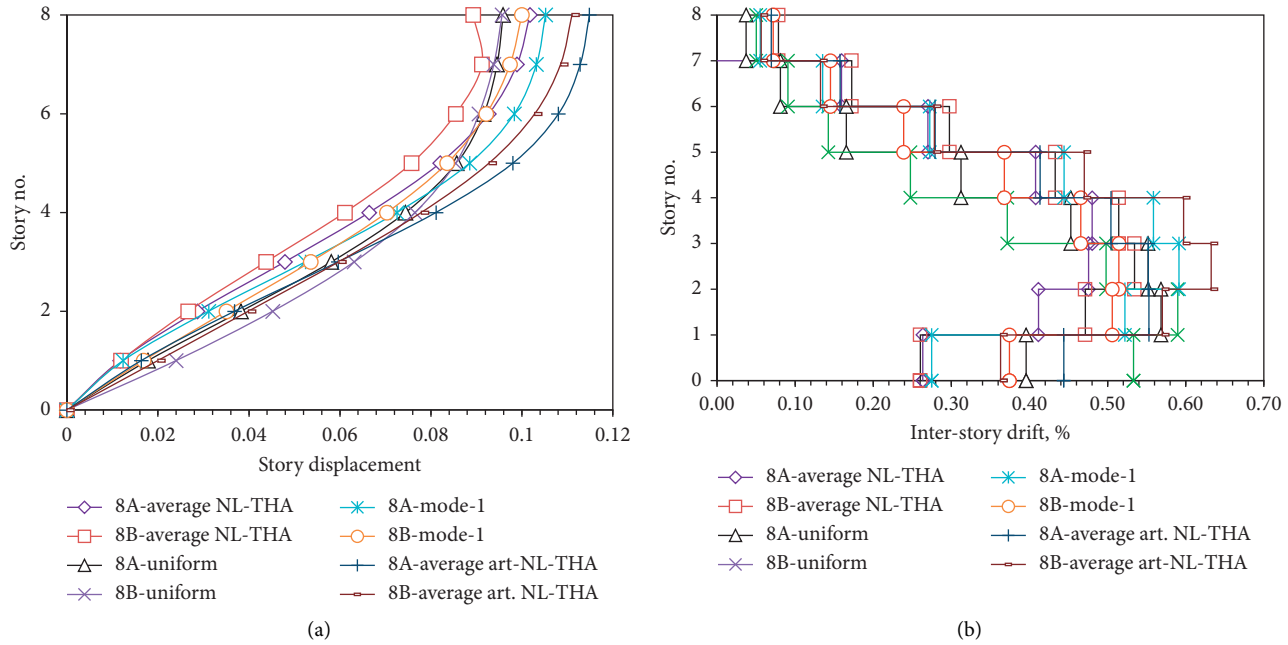

Figure 8: (a) Roof drift and (b) interstory drift for 8-story frame of 8A and 8B model frames.

The results of the static and dynamic analyses were also compared in terms of displacement and interstory drift for equal roof drift of 0.34% (0.10 m roof displacement) in SPO and the average value obtained from NL-THAs analysis from the real earthquake records and synthetic earthquake scaled to the design PGA = 0.3 g for matched ground motion (Figure 6) reference to soil II-GB11-10. In Figures 8(a) and 8(b), the static and dynamic average drift analyses along the height of the frame are shown. Figure 8(a) displays that the displacement diagram obtained with the modal shape and with the dynamic analyses resulted very similar. The modal shape caused values slightly larger than the dynamic analyses at the upper floors. The pushover analysis with uniform load shape produced a different displacement diagram, with much larger values than the other methods of analysis at the first floors for 8B model followed by 8A uniform. In both NL-THA and SPO analyses, 8B interstory gives larger value than 8A at the bottom story, whereas 8A Art-NL-THA and 8A-Mode-1 give larger value in the second and third floors. Moreover, in major cases, the SPO and NL-THA analyses are consistent in which average NL-THA interstory drifts are closer to Mode-1 in both models that allow the use of SPO analysis [31, 58].

Moreover, Figure 9 shows the qualitative comparison of plastic hinge locations and formations of both models determined by SPO and NL-THA analyses. For single artificial acceleration scaled to 0.6 g, NL-THA analysis results of 0.20 m roof displacement (0.67% roof drift) with equal 0.67% roof drifts in SPO plastic hinge patterns are compared. In the NL-THA analysis, the plastic hinges are well distributed along the height of the frame, while for SPO, more hinges occur in lower stories. Yet, for the same 0.67% roof drift in both 8A and 8B model frames, Figures 9(a)–9(f) show the bottom story column hinge formation in SPO is nearly consistent to NL-THA though disparity is observed in beam hinges. For NL-THA analysis, in all cases, more beam hinge yielding is noted in 8A than 8B model for IO level (immediate occupancy, Figure 5), whereas column hinge formation is more in 8B than 8A columns. It highlights the energy dissipation mechanism differences in the two designed models.

Nevertheless, the above brief illustrative example for 8-story frame gives useful insight, in which the SPO analysis results are consistent with the NL-THA analysis that could confirm the validity of SPO analysis for the considered model.

5.2. Pushover Curve. Figures 10(a)–10(c) represent the pushover (capacity) curves of 4-, 8-, and 12-story RC frames designed with ES8-15 and GB11-10. For all models and lateral load pattern, the curve is nearly the same at the beginning as the concrete cross-sections are equal. However, beyond the elastic range, the capacity curves show different results. The pushover analysis using the uniform lateral load pattern yielded a higher initial stiffness and base shear capacity as compared with Mode 1. In other words, for the same base shear force, the uniform load pattern had a lower roof displacement. This is due to differences in the lateral displacement in the upper stories, where the Mode-1 load pattern resulted in higher displacements. Certainly, the 'Uniform' loading pattern resulted in the highest elastic stiffness and peak strength in all structures for both codes. However, FEMA 356 [6] recommends the most critical lateral load pattern should be considered in the evaluation process of all elements, while ES8-15 recommends a load pattern with a smaller over-strength ratio obtained from corresponding pushover curves.

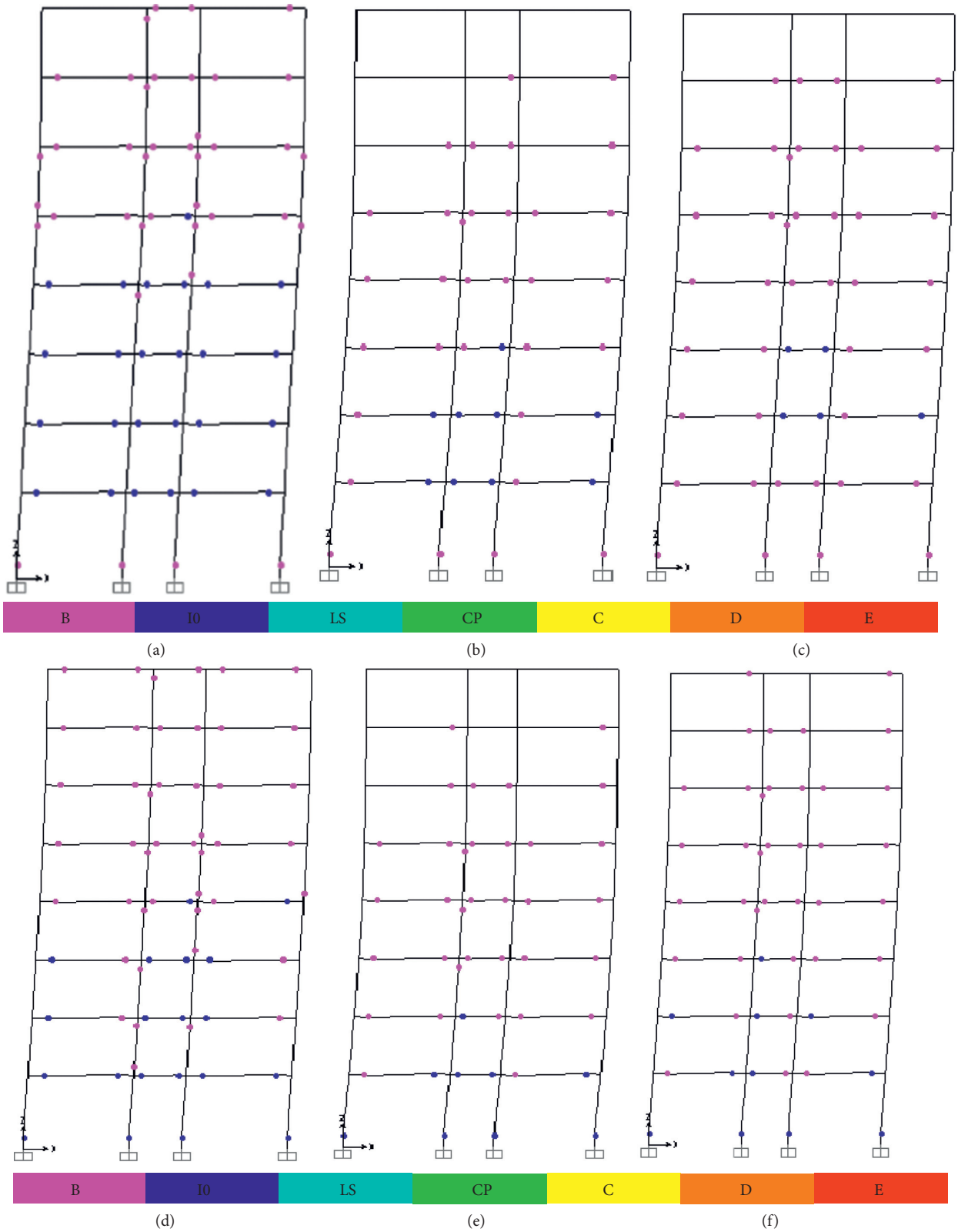

Figure 9: State of the plastic hinges in Models 8A and 8B: NL-THA and SPO analyses. (a) 8A-NL-THA. (b) 8A-SPO Uniform. (c) 8A-SPO-Mode-1. (d) 8B-NL-THA. (e) 8B-SPO Uniform. (f) 8B-SPO-Mode-1.

Moreover, the capacity curves of the models differ among ES8-15 and GB11-10 designed ones except for the 4-story frame. Both codes 4-story frame pushover curves show closer values. However, the yield displacement for the frame designed with GB11-10 is smaller than ES8-15. Thus, for a specified ultimate roof displacement, a little higher ductility

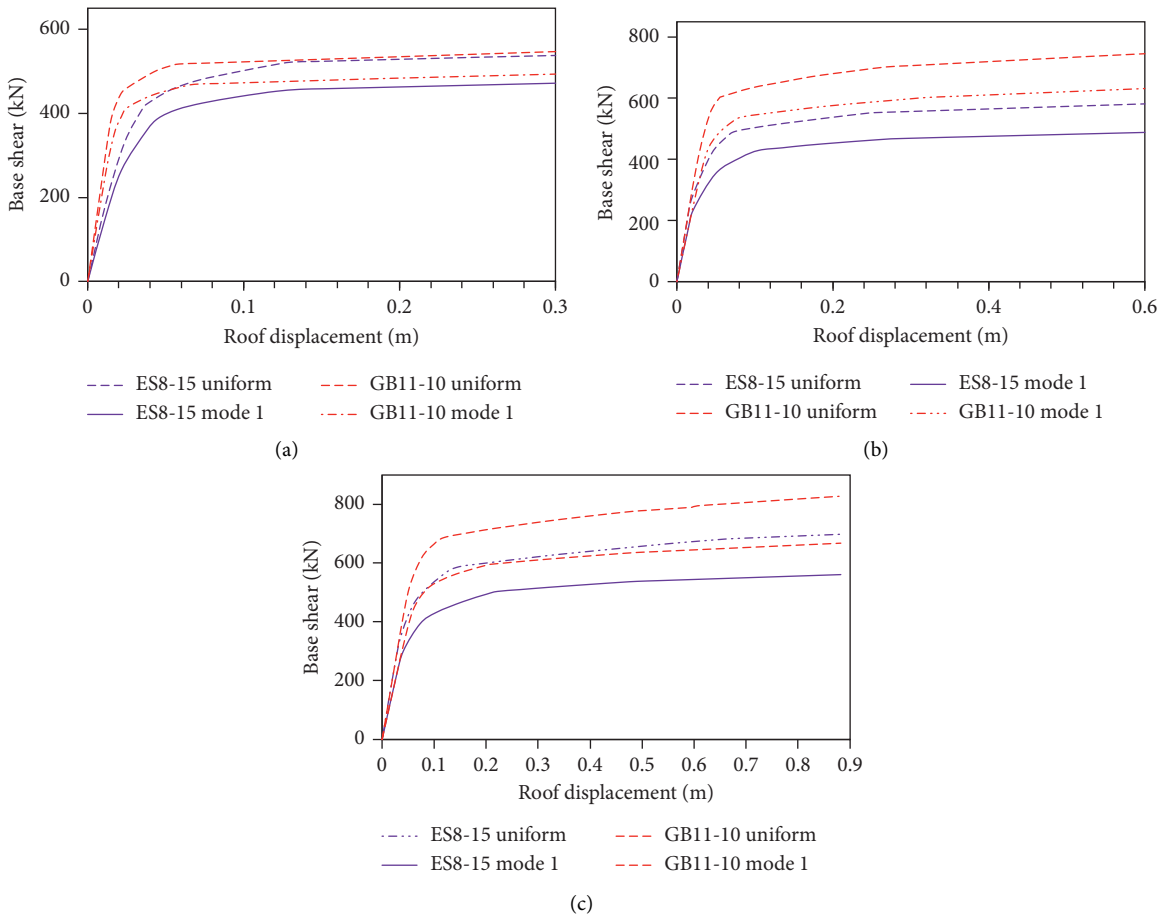

Figure 10: Pushover curves: (a) 4-story, (b) 8-story, and (c) 12-story frames.

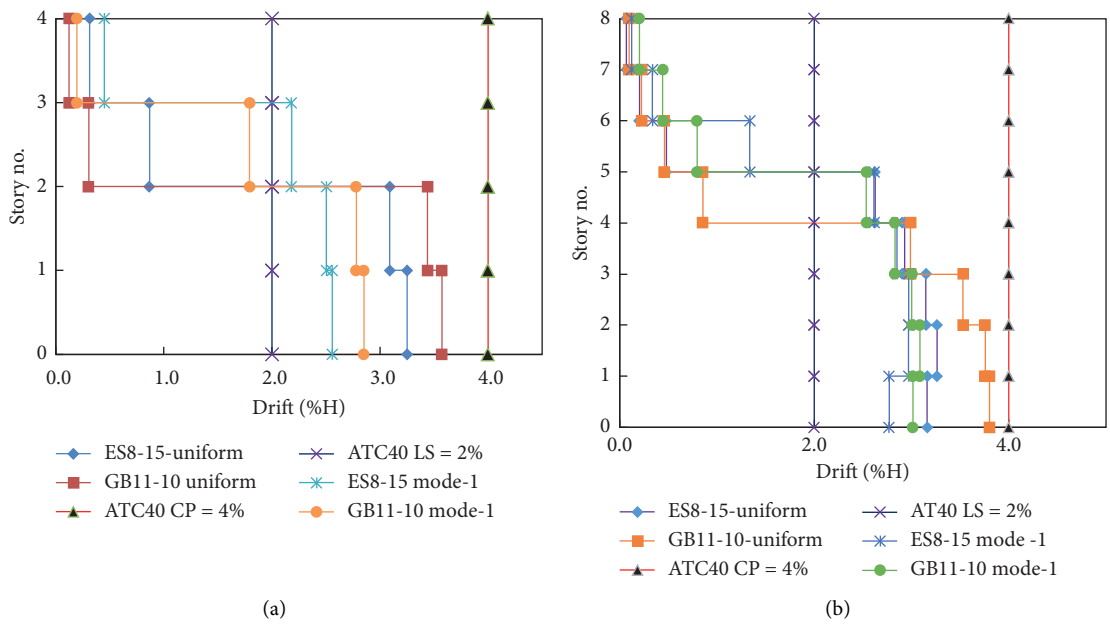

Figure 11: Continued.

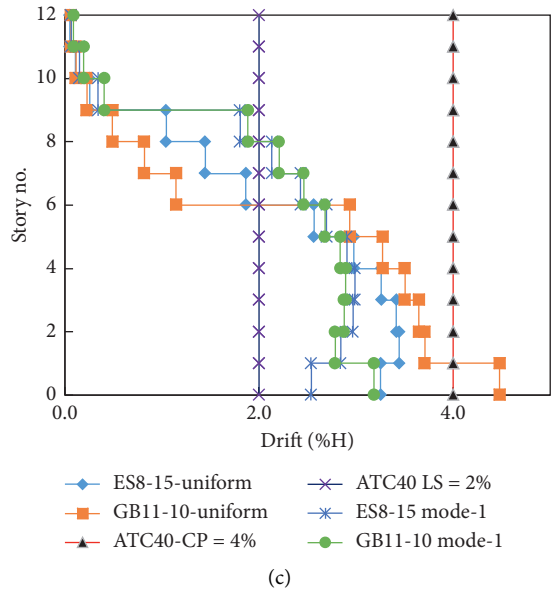

(c)

Figure 11: Interstory drift: (a) 4-story, (b) 8-story, and (c) 12-story frames.

may be attained for low-rise RC moment frames designed with GB11-10. In all other cases, many more differences among the capacity curves are observed. Such differences are remarkable for 8- and 12-story models and are generally attributed to the way that the codes distribute the strength (and hence stiffness) among the structural members of the structure. Particularly, Figures 10(b) and 10(c) show that notable differences among the peak strengths attained 8- and 12-story models designed with ES8-15 and GB11-10, respectively. For uniform load pattern, the peak strength of the models designed with GB11-10 is approximately 744 kN and 827 kN compared with 581 kN and 698 kN values for the model designed with ES8-15 in 8- and 12-story models, respectively. However, as will be shown later, the lower peak strength capacity of structures designed with ES8-15 does not have severe significant effects on their overall performance.

5.3. Interstory Drift. The interstory drift ratio is critical for seismic performance evaluation, as it is directly related to the level of structural damage. It is calculated as the difference in lateral displacement between two adjacent floor levels normalized by the corresponding story height. ATC 40 suggests typical limits of 2% interstory drift associated with life safety (LS) performance level and 4% interstory drift for collapse prevention (CP) performance [7]. Figures 11(a)–11(c) display the interstory drift of the model frames. As expected, the uniform load pattern leads to a more distinct soft-story behavior at the first story, particularly for GB11-10 designed structure in all 4-, 8-, and 12-story frames than Mode 1. In all frames, Figures 11(a) to 11(b), the interstory drift exceeds the life safety level of ATC 40 until the mid-height of each model frames in both codes. Besides, in Figure 11(c), the 12-Story GB11-10 designed frame passes the collapse prevention (CP) level at the bottom story. This indicates that the first story has the potential to act as a soft story under significant seismic load in GB11-10. Nevertheless, in the top stories, the reverse is happening for Mode-1. Mode-1 interstory drift in most cases' frames designed by ES8-15 is more than GB11-10 above the midheight of the model frames than the uniform load pattern. However, this may not be critical as bottom stories with more axial force may initiate buckling. It shows that ES8-15 is better than GB11-10 in the assignment of stiffness and strength in the design of the structures.

Additionally, observing the sharp drop of interstory drift in the midstory in all models of GB11-10, one can ask a legitimate question. It is directly related to the plastic hinge formation sequence and distribution in columns and beams that vary as per the capacity designed for plastic hinges at beam-column joints of the models. As noted earlier in the design (Section 3), all the beam-column joints confirm the minimum strong column-weak beam capacity ratio. Thus, it may be difficult to make a conclusion whether GB11-10 designed frames satisfy or not the seismic ground motion in nonlinear range until the performance point assessment analysis (Section 5.4) is made. The 2% roof drift may be beyond the design limit. Likewise, it has to be noted that one main aim of seismic performance analysis is to discover a weakness that might appear in the design. Neverthless, it is undeniable that ES8-15 ductility is little more than GB11-10 in the aforementioned comparisons.

5.4. Plastic Hinge Formation. Figure 12 (I) to (IV) illustrate the sequence and locations where those plastic rotation limits exceeded in beams and columns as per the plastic hinge definition in Figure 5 for immediate occupancy (IO), life safety (LS), and collapse prevention (CP). All the figures show a deformed frame with plastic hinges at the final push steps with roof displacement of 2% of roof drifts noted in

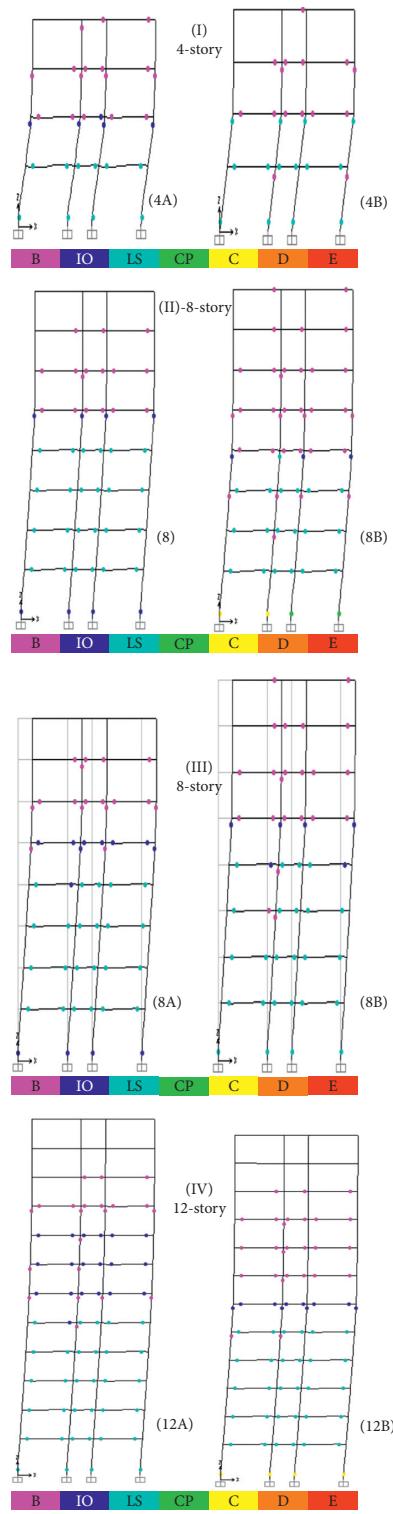

Figure 12: State of the plastic hinges in 4 (I-Uniform), 8 (II-Uniform, III-Uniform, and Mode 1), and 12 (III-Uniform): Left Model (A)-ES8-15 and Right Model (B)-GB11-10 Model Frames.

Section 4 for the uniform load pattern. Mode-1 load pattern deformed shape and intermediate steps are not shown for space limitation except the 8-story frame. Figure 12 (I) shows the state of the plastic hinges of the 4-story model designed according to both codes (A) ES8-15 and (B) GB11-10. For the structures designed using both codes with all load patterns, the plastic hinges were typically formed at the lower part of the structure. In addition, in most cases, plastic hinging was initiated from the first-story columns hinges (at the base) when a uniform lateral load pattern was applied to the structure. The trends mentioned above were also observed for all models with different numbers of

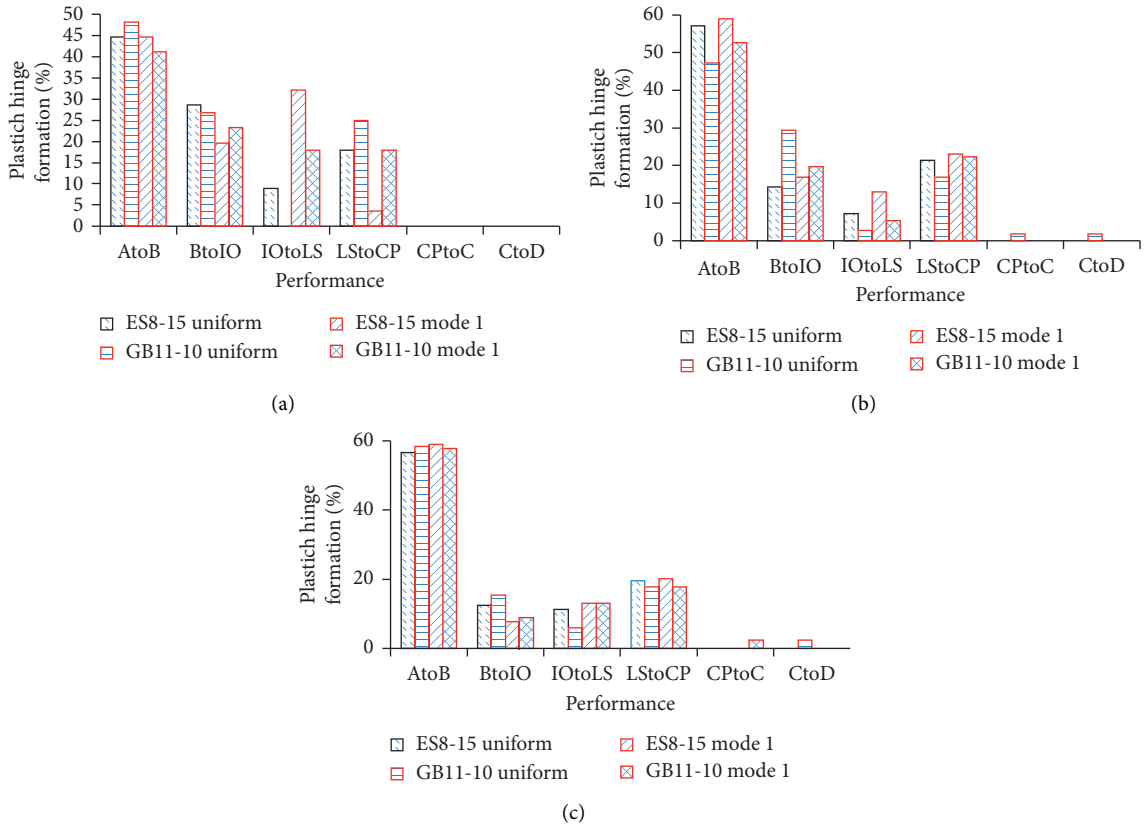

Figure 13: Total number of plastic hinges (%) formed: (a) 4-story, (b) 8-story, and (c) 12-story.

stories. Although few plastic hinges have formed in the columns Figure 12 (I) to (IV), generally for all structures, the beam-sway mechanism was the dominant mechanism rather than the column-sway mechanism, showing the design met intended strong-column/weak-beam provision except few cases. Plastic hinges at column bases were found to be more critical for all structures designed with GB11-10 than with the ES8-15. Figure 12 (II and III) shows the hinge pattern for the 8-story model frame. ES8-15-designed frame columns are within the IO level noted in the 1st floor and 4th floor as compared with GB11-10 with CP and collapse at 1st floor and 3rd floor LS and IO levels. Figure 12 (III) Mode-1 shows a similar trend to the uniform load pattern. This shows a better performance of ES8-15-designed frames.

In the same way, Figure 12 (IV) illustrates a plastic hinge pattern for the 12-story model frame and ES8-15(A)-designed frame shows that a beam mechanism with only 4 columns is within the LS level noted in the 1st floor and remaining few with the elastic range in 4 and above 4 stories. In addition, the beams' plastic hinges are well distributed; bottom stories-LS, middle stories-IO, and top stories-elastic. However, for the GB11-10-designed 12-story model, 4-column exhibits collapse in the 1st floor and 5th Floor, 4 columns LS, and remaining elastic. In the case of beams for GB11-10-designed 12-story frame up to midstory show LS as ES8-15; however, the remaining IO is at one midfloor only, remaining elastic. In summary, the plastic hinges of columns in GB11-10 structures occur more in number and reach to life safety and collapse level earlier than ES8-15 for all structures subjected to equal roof displacement. In addition, the plastic hinge formation occurs more early in the beams than columns for ES8-15-designed structures as compared with GB11-10-designed ones. It proves that a strong-column–weak-beam is maintained in the ES8-15 design. This confirms that the stiffness distribution is good in ES8-15, as noted in [8]. As it was mentioned earlier, the interstory drift profiles showed that GB11-10-designed frames have larger drift at collapse than ES8-15 particularly for 8- and 12-story models. This demonstrates that a larger capacity curve (strength) in Section 5.2 does not mean better seismic performance [3].

Figures 13(a)–13(c) show the performance evaluations of all frames designed with the two codes. The figures represent the number of plastic hinges that fall within specific performance limits, namely, fully elastic (A to B in the figures), IO (B to IO), LS (IO to LS), CP (LS to CP), and beyond the collapse (CP to C or C to E), as per the definitions shown in Figure 5. They also show the total number of hinges formed in the model as the structures pushed gradually to a 2% target displacement roof drift. The percentage of hinge formation is bigger in IO (B to IO) than other limits. For all frames designed by ES8-15 fall within collapse prevention limits, for GB11-10a, nearly 3% exceeds the collapse prevention limits for 8- and 12-story frames. Generally, hinges with the uniform lateral pattern are more critical than Mode-1.

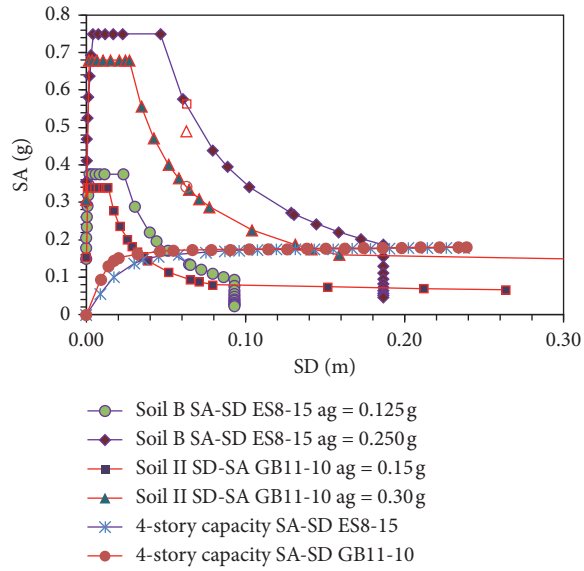

Figure 14: ADRS Response spectra and capacity curve for ES8-15 and GB11-10.

Table 5: Target displacement (in cm) capacity spectrum method ATC-40 and N2 (ES8-15).

Load pattern	Seismic code	PGA	4-story		8-story		12-story	
			ATC 40	N2	ATC 40	N2	ATC 40	N2
Uniform	ES8-15	0.125 g	5.50	5.57	9.40	9.33	9.30	9.30
		0.25 g	11.00	11.13	18.60	18.66	18.70	18.60
	GB11-10	0.15 g	3.40	3.65	8.10	8.97	16.00	17.31
		0.30 g	7.00	7.30	16.00	16.61	35.00	34.62
Mode-1	ES8-15	0.125 g	5.69	6.32	10.98	11.67	11.36	9.25
		0.25 g	12.00	12.65	22.49	24.39	24.93	18.50
	GB11-10	0.15 g	4.04	4.06	9.15	10.85	18.58	18.27
		0.30 g	8.78	8.12	19.61	21.80	37.17	36.13

5.5. Performance Point Analysis. ATC 40 defines the performance point as the maximum structural displacement expected for the demand ground motion due to an earthquake. The seismic demand is given by the amount of displacement at the performance point in the capacity spectrum method of ATC 40. Member displacement and forces are computed at this displacement and are used as the inelastic demand and checked against the available capacities of members. The performance point is one of the fundamental goals of this study to evaluate the seismic performance of buildings designed as per ES8-15 and GB11-10. For the performance point analysis, we chose simplified methods based on their relative accuracy to that of the nonlinear dynamic analysis approach. The procedures of ATC-40 provided values very close to the average dynamic analysis results [51, 52].

As a result, ATC 40 and N2 in ES8-15 are used to evaluate the performance point with respective seismic demand with ground acceleration 0.15 g and 0.30 g in terms of an equivalent response spectrum of ES8-15 and GB11-10. It is done based on the capacity curve (pushover curves) of each model frame presented in the previous sections being converted to the equivalent single degree of freedom by transformation factor procedures laid out in N2 and ATC 40. As an example, Figure 14 shows the transformed acceleration-displacement capacity curve for a 4-story of Mode-1 lateral load pattern. The demand acceleration-displacement response spectrum (ADRS) for $a_g = 0.15$ g and 0.30 g soil group II in GB11-10 and equivalent soil B in ES8-15 is shown in Figure 9. Converting the elastic acceleration-period spectrum uses the equation $S_D = S_A(T) * (T/2\pi)^2$ and $S_e(T)$. Figure 14 shows, for $a_g = 0.125$ g and 0.25 g (reference to soil class A), nearly at $S_D = 0.093$ m and 0.190 m, respectively, the S_A of ES8-15 is a constant value, while GB11-10 shows a different way, that may influence the performance assessment.

Table 5 shows the summarized results of the target displacements calculated for the two lateral load patterns in all models that display both methods give nearly the same value. It is interesting to note that, in all cases, target displacements based on the 'uniform' load pattern are less than with Mode-1 as expected. Furthermore, Table 6 shows a summary of target displacement and base shear with ATC 40. In all cases, the base shear within GB11-10 is greater than ES8-15 by 5%, 4%, and 34%, respectively, in 4-, 8-, and 12-story model buildings, for uniform load patterns with PGA of $a_g = 0.15$ g. Similarly, 2%, 12%, and 26% are for PGA $a_g = 0.3$ g ground motion. Conversely, the target

Table 6: Target displacements and base shear calculated using the capacity spectrum method ATC 40.

Lateral load pattern	Seismic code	PGA	4-story		8-story		12-story	
			Dt (cm)	V (kN)	Dt (cm)	V (kN)	Dt (cm)	V (kN)
Uniform	ES8-15	0.125 g	5.5	457.89	9.4	500.18	9.3	521.46
		0.25 g	11.0	508.58	18.6	533.26	18.7	596.95
	GB11-10	0.15 g	3.4	479.87	8.1	521.46	16.0	701.14
		0.30 g	7.0	518.63	16.0	596.95	35.0	750.38
Mode-1	ES8-15	0.125 g	5.7	408.10	11.0	430.83	11.4	439.10
		0.250 g	12.0	451.82	22.5	458.05	24.9	507.82
	GB11-10	0.15 g	4.0	441.60	9.2	541.51	18.6	585.79
		0.30 g	8.8	471.17	19.6	575.21	37.2	621.03

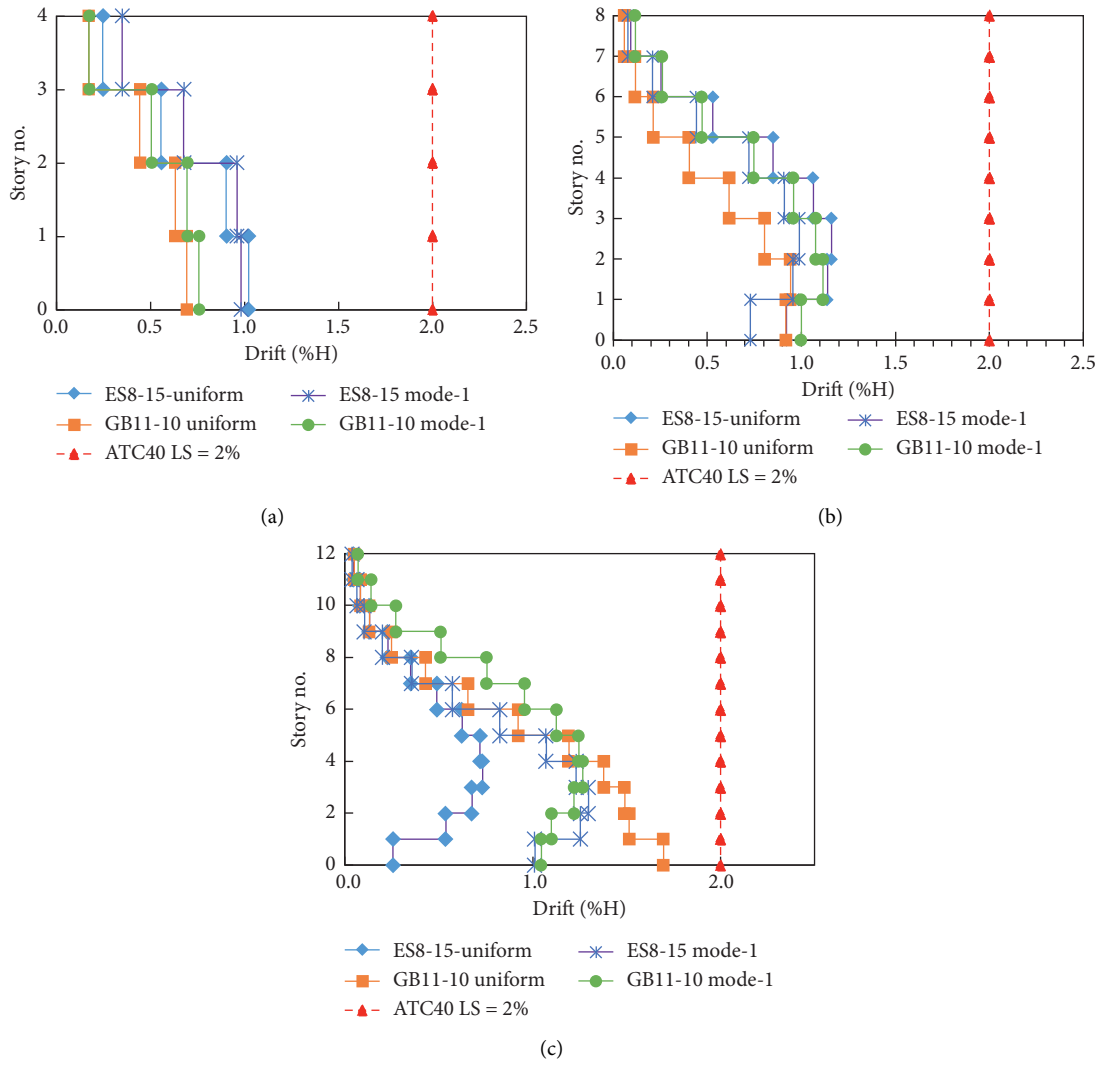

Figure 15: Interstory drift (a) 4-, (b) 8-, and (c) 12-story at performance point at $a_g = 0.30$ g.

displacement in ES8-15 is greater than GB11-10 by 36% and 14% in 4- and 8-story models, respectively, for a uniform load pattern for PGA values of 0.15 g and 0.3 g. Likewise, 28% and 13% are for Mode 1 load pattern. Nevertheless, a 12-story target displacement in ES8-15 is smaller by 22% to 34% in Mode 1 and the uniform load pattern. This discloses the seismic performance is becoming more different as the story number increases within the two codes. Besides, at the performance point of all models, the global roof drift at the control node is less than 2% height of building satisfying the life safety roof drift limits stated in ATC 40. For ground acceleration, PGA = 0.30 g, Mode-1 load pattern being 0.78%, 0.75%, and 0.56%, respectively, for 4-, 8-, and 12-story in ES8-15. In the same way, 0.58%, 0.65%, and 0.84%, respectively, in GB11-10-designed frames. This demonstrates the roof drift is increasing with building height in GB11-10

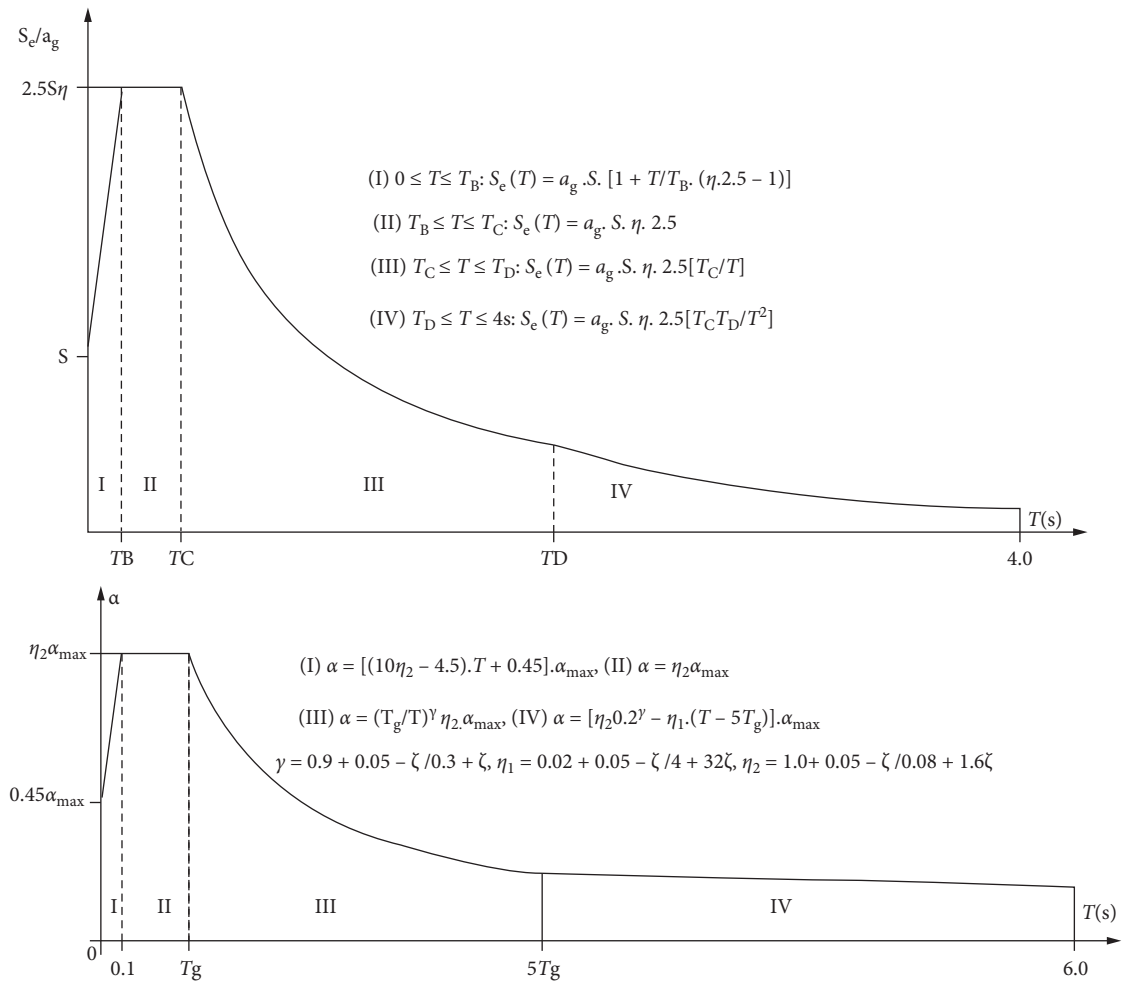

Figure 16: Design response spectrum provisions: (a) Ethiopia-ES8-15 and (b) Chinese GB11-10.

while decreasing in ES8-15 designed frames as the consequence of their respective spectrum provision, although ES8-15 has better deformation capacity as noted earlier.

Moreover, Figure 15 illustrates interstory drift in 4-, 8-, and 12-story frames satisfying 2% life safety level in ATC 40 at performance point for ground motion 0.3 g. It is another way of proving that the design frames' roof drift is below 2%, for which the designed members' performance need to be checked against the design. For 4-story frame, ES8-15-designed frames show larger interstory drift than the corresponding GB11-10. However, for 8-story one, the interstory drift is nearly equal in both cases. On the other hand, for 12-Story one, GB11-10 gives larger interstory drift at the bottom story than ES8-15. Such dissimilarities of interstory drift with 4-, 8-, and 12-story models are associated with the respective codes' elastic demand spectrum, although the structural performance of ES8-15 designed frames are better than GB11-10. The period of vibration of the structure increases in the nonlinear range due to stiffness degradation. As noted in Figure 14, the demand spectrum of GB11-10 becomes higher than that of ES8-15, particularly for the period of vibration $T > 2.0$ s. Such big differences can lead to an underestimation of responses in ES8-15(EN1998-1) as shown in [59, 60], which in turn affects other structure responses [52].

6. Conclusions

This research examined the seismic performance of RC moment-resisting frame design as per the Ethiopian (ES8-15 based on European Norm EN1998-1) and the Chinese (GB11-10) seismic codes. The study considered 4-, 8-, and 12-story RC model frames, which are designed with the capacity design principle in the two codes. The obtained design results displays the existence of differences in the allocation of reinforcement among the column and beam in the frames; despite this, the total reinforcement (rebar) in the frames are nearly equal. Following the design, the model frame seismic performances are evaluated via nonlinear static (pushover) procedures stated in FEMA 356, ATC 40 documents, and provisions in the respective codes of ES8-15 and GB11-10. Besides, for the 8-story frame, illustrative nonlinear time history analysis also has been made and confirms the good agreement with pushover analysis. The seismic performance analysis disclosed many interesting similarities of the two codes. Conversely, some essential discrepancies are also noted and are summarized in the following ways:

(1) Pushover analysis up to 2% roof drift as per ATC 40 life safety provision structural performances

Table 7: Seismic intensity, PGA, and α_{max} maximum seismic influence coefficient GB11-10 [15, 23].

Chinese seismic intensity	6	7		8		9
PGA zone	<0.10 g	0.10 g	0.15 g	0.20 g	0.30 g	≥0.40 g
Frequent earthquake	0.04	0.08	0.12	0.16	0.24	0.32
Moderate earthquake	0.12	0.23	0.34	0.45	0.68	0.90
Rare earthquake	0.28	0.50	0.72	0.90	1.20	1.40

Table 8: Site classes equivalence of ES8-15 and GB11-10.

Shear velocity range		Soil class	
GB11-10	ES8-15	GB11-10	ES8-15
500 ≤ vs < 800	>800	I_0	A
		I_1	
250 ≤ vs < 500	360 ≤ vs < 800	II	B
150 ≤ vs < 250	180 ≤ vs < 360	III	C
<150	<180	IV	D

Table 9: ES8-15 values of corner period T and soil amplification factor Type 1 ($M \geq 5.5$) and Type 2 ($M < 5.5$).

Ground type	S		TB(s)		TC(s)		TD(s)	
	Type-1	Type-2	Type-1	Type-2	Type-1	Type-2	Type-1	Type-2
A	1.00	1.000	0.15	0.050	0.40	0.250	2.0	1.2
B	1.20	1.350	0.15	0.050	0.50	0.250	2.0	1.2
C	1.15	1.500	0.20	0.100	0.60	0.250	2.0	1.2
D	1.35	1.800	0.20	0.100	0.80	0.300	2.0	1.2

(i) GB11-10-designed frames show a larger push-over capacity curve; however, more plastic hinges form in the columns that affect interstory drifts.

(ii) In ES8-15-designed frames, more plastic hinges (energy dissipation) form in beams than in the columns, which exhibit better strong-column–weak-beam scenario, also distributed uniformly along with the height of the structure.

(2) Pushover analysis with the roof drift up to the performance point (target displacement)

(i) The performance point analysis shows the target displacement in ES8-15 is greater than GB11-10 with smaller height frames 4- and 8-story but becomes less for the 12-story frame.

(ii) These variations are directly associated with the codes' elastic spectrum uniqueness, and the demand spectrum of GB11-10 is considerably larger than of ES8-15, particularly for $T > 2.0$ s

(3) For the aforementioned arguments in (1) and (2), it has to be noted that the performance point analysis (2) in both codes satisfy the design requirement; nonetheless, their structural performances discrepancy is 2% roof drift in (1), which is beyond their expected design limit; nevertheless, these are the important witnesses for the benefits gained while comparing various seismic codes as they have their own merits over one another.

(4) To sum up, despite the present study is limited to RC moment-resisting frames, mainly non-linear static analysis, it shows interesting insight to extend such researches for various types of structures with different analysis methods for further investigation of the two codes' weaknesses and strengths.

Appendix

A. Response Spectrum Provisions of Ethiopian and Chinese Seismic Codes

Response Spectrum Provisions of Ethiopian and Chinese Seismic Codes are given below (Figure 16).

(1) For ES8-15 (a)

$S_e(T)$ is the elastic response spectrum

T is the vibration period of a linear single-degree-of-freedom system

a_g is the design ground acceleration on type A ground ($a_g = \gamma_{Io} a_{gR}$) for seismic hazard of map of Ethiopia given in Appendix-D of Ethiopia Seismic Code Standard, ES8-15

T_B is the lower limit of the period of the constant spectral acceleration branch

T_C is the upper limit of the period of the constant spectral acceleration branch

T_D is the value defining the beginning of the constant displacement response range of the spectrum

S is the soil factor

η is the damping correction factor with a reference value of $\eta = 1$ for 5% viscous damping

Table 10: GB11-10 corner period(s) for earthquake design group and soil type.

Site soil condition type	Design earthquake group-1		Design earthquake group-2		Design earthquake group-3	
	T_g	$5T_g$	T_g	$5T_g$	T_g	$5T_g$
Io	0.20	1.00	0.25	1.25	0.30	1.50
I1	0.25	1.25	0.30	1.50	0.35	1.75
II	0.35	1.75	0.40	2.00	0.45	2.25
III	0.45	2.25	0.55	2.75	0.65	3.25
IV	0.65	3.75	0.75	3.75	0.90	4.50

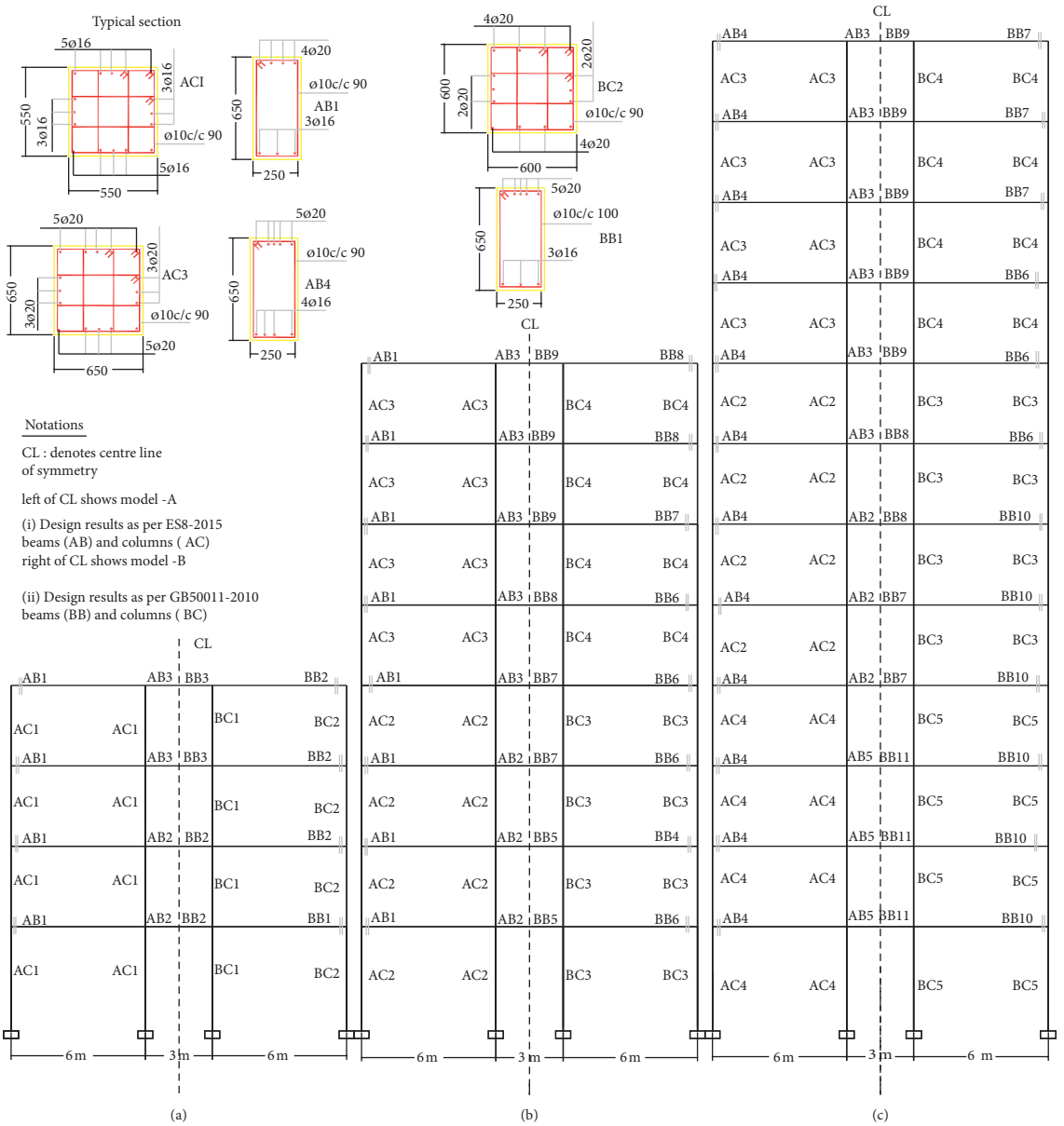

Figure 17: Reinforcement design diagram for (a) 4-, (b) 8-, and (c) 12-story RC frame designed as per ES8-15 and GB11-10.

(2) For GB11-10 (b)

α-design seismic influence coefficient

T-period of vibration for single-degree-of-freedom system

α_{max} is maximum of earthquake affecting coefficient that depends on design level of GB11-10

ζ is the damping ratio and $\eta_2 \geq 0.55$

γ is the attenuation index

Table 11: Beam and column section design.

Cross type	Building-A ES8-15						Building-B GB11-10		
	Cross section	Rebar top (T) bottom (B)	Stirrup (mm)	Cross section	Rebar top (T) bottom (B)	Stirrup (mm)	Cross section	Rebar top (T) bottom (B)	Stirrup (mm)
Beam	AB1-25 × 65	4Φ20(T) 3Φ16(B)	90	BB1-25 × 65	5Φ20(T) 3Φ16(B)	100	BB7-25 × 65	4Φ20(T) 4Φ16(B)	90
	AB2-25 × 65	4Φ16(T) 3Φ16(B)	90	BB2-25 × 65	4Φ20(T) 3Φ16(B)	100	BB8-25 × 65	3Φ20(T) 4Φ16(B)	90
	A B3-25 × 65	3Φ16(T) 3Φ16(B)	90	BB3-25 × 65	3Φ16(T) 3Φ16(B)	100	BB9-25 × 65	4Φ16(T) 4Φ16(B)	90
	AB4-25 × 65	5Φ20(T) 3Φ20(B)	90	BB4-25 × 65	6Φ20(T) 4Φ16(B)	100	BB10-25 × 65	6Φ20(T) 5Φ16(B)	90
	AB5-25 × 65	3Φ20(T) 3Φ16(B)	90	BB5-25 × 65	5Φ20(T) 3Φ20(B)	100	BB11-25 × 65	5Φ20(T) 5Φ16(B)	90
				BB6-25 × 65	5Φ20(T) 4Φ16(B)	100			
Column	AC1-55 × 55	16Φ16	90	BC1-55 × 55	16Φ16	100			
	AC2-60 × 60	16Φ20	40	BC2-55 × 55	12Φ16	100			
	AC3-55 × 55	12Φ20	90	BC3-60 × 60	12Φ20	100			
	AC4-65 × 65	16Φ20	40	BC4-55 × 55	12Φ20	100			
				BC5-65 × 65	14Φ20	100			

η_1 is the adjustment coefficient for descending slope in the linear decreasing section

η_2 is the damping adjustment coefficient

(3) Design (inelastic) response spectrum (Ethiopian ES8-15) in addition to elastic one for regions I, II, IV, and V:

$$\text{(I) } S_d(T) = a_g \cdot S \cdot \left[\frac{2}{3} + \frac{T}{T_B} \cdot \left(\frac{2.5}{q} - \frac{2}{3}\right)\right],$$

$$\text{(II) } S_0(T) = a_g \cdot S \cdot \frac{2.5}{q},$$

$$\text{(III) } S_0(T) = \begin{cases} = a_g \cdot S \cdot \dfrac{2.5}{q} \cdot \left[\dfrac{T_C}{T}\right] \\ \\ \geq \beta \cdot a_g, \end{cases} \tag{A.1}$$

$$\text{(IV) } S_0(T) = \begin{cases} = a_g \cdot S \cdot \dfrac{2.5}{q} \cdot \left[\dfrac{T_C \cdot T_D}{T^2}\right] \\ \\ \geq \beta \cdot a_g, \end{cases}$$

where q is the behavior factor accounting for ductility and energy dissipation, $\beta \geq 0.2$, and $S_e(T)$, T, a_g, T_B, T_C, and S are defined above (Tables 7–10).

B. Design Detail Drawing and Table

Design detail drawing and table are given in Figure 17 and Table 11.

Data Availability

The data used to support the findings of this study are included within the article.

Conflicts of Interest

The authors declare that they have no conflicts of interest.

Acknowledgments

This study was supported by the China Scholarship Council (CSC), Grant No. CSC2016DFH241, and the Natural Science Foundation of China, Grant No 51579139, while conducting the study in Three Gorges University, China. The first author also thanks his institution Jimma University in Ethiopia for receiving additional support.

References

[1] V. N. Khose, Y. Singh, and D. H. Lang, "A comparative study of design base shear for RC buildings in selected seismic design codes," *Earthquake Spectra*, vol. 28, no. 3, pp. 1047–1070, 2012.

[2] M. Zameeruddin and K. K. Sangle, "Review on recent developments in the performance-based seismic design of reinforced concrete structures," *Structures*, vol. 6, pp. 119–133, 2016.

[3] M. J. N. Priestley, "Performance based seismic design," in *Proceedings of the 12th World Conference on Earthquake Engineering*, Auckland, New Zealand, 2000.

[4] S. L. Kramer, "Performance-based design methodologies for geotechnical earthquake engineering," *Bulletin of Earthquake Engineering*, vol. 12, no. 3, pp. 1049–1070, 2014.

[5] A. Ghobarah, "Performance-based design in earthquake engineering: state of development," *Engineering Structures*, vol. 23, no. 8, pp. 878–884, 2001.

[6] Federal Emergency Management Agency, *FEMA 356: Prestandard and Commentary for the Seismic Rehabilitation of Buildings*, Federal Emergency Management Agency (FEMA), Washington, DC, USA, 2000.

[7] Applied Technology Council, *ATC-40: Seismic Evaluation and Retrofit of Concrete Buildings*, Vol. 1-2, Applied Technology Council (ATC), Redwood City, CA, USA, 1996.

[8] A. Kiani, S. Manie, and B. Mansouri, "Comparison of code-specific non-linear seismic performance," *Proceedings of the Institution of Civil Engineers-Structures and Buildings*, vol. 169, no. 7, pp. 471–491, 2016.

[9] G. Shi, F. Hu, and Y. Shi, "Comparison of seismic design for steel moment frames in Europe, the United States, Japan and China," *Journal of Constructional Steel Research*, vol. 127, pp. 41–53, 2016.

[10] C. A. Zeris and C. C. Repapis, "Comparison of the seismic performance of existing RC buildings designed to different codes," *Earthquakes and Structures*, vol. 14, no. 6, pp. 505–523, 2018.

[11] D. Taye, "Tsehay real estate inaugurates apartment buildings," in *All Africa*, Tsehay Real Estate Plc, Addis Ababa, Ethiopia, 2014, https://allafrica.com/stories/201409220989.html.

[12] R. Sweet, "21-tower scheme to be Ethiopia's "biggest real estate project" says Chinese developer," in *Global Construction Review*, Website of the Chartered Institute of Building, Bracknell, England, UK, 2015, http://www.globalconstructionreview.com/news/21-tower-scheme-be-et8hio0pias6-4b2ig5gest0-r8ea/.

[13] Xinhua, Chinese Company to Build Tallest Building in East Africa, 2015, http://www.chinadaily.com.cn/business/2015-04/29/content_20580309.htm.

[14] X. Jin and J. Zhao, "Development of the design code for building structures in China," *Structural Engineering International*, vol. 22, no. 2, pp. 195–201, 2012.

[15] China Ministry of Construction, *GB50011-2010: China Code for Seismic Design of Buildings*, China Architecture and Building Press, China Ministry of Construction, Beijing, China, 2010.

[16] Y. X. Hu, "Development of earthquake engineering in China," in *Proceedings of the World Conference on Earthquake Engineering*, Vancouver, Canada, August 2004.

[17] A. Ayele, "Probabilistic seismic hazard analysis (PSHA) for Ethiopia and the neighboring region," *Journal of African Earth Sciences*, vol. 134, pp. 257–264, 2017.

[18] Z. Lubkowski, M. Villani, K. Coates, N. Jirouskova, and M. Willis, "Seismic design considerations for East Africa," in *Proceedings of the European Conference on Earthquake Engineering and Seismology*, Istanbul, Turkey, August 2014.

[19] E. Booth, "Dealing with earthquakes: the practice of seismic engineering "as if people mattered"," *Bulletin of Earthquake Engineering*, vol. 16, no. 4, pp. 1661–1724, 2018.

[20] Ethiopia Ministry of Construction, *ES8-2015: Ethiopian Standard 8 Based Euro Norms; Design of Earthquake Structures for Earthquake Resistance_Part 1: General Rules_Seismic Actions and Rules for Buildings*, Ethiopia Ministry of Construction, Addis Ababa, Ethiopia, 2015.

[21] S. Hicks, "Eurocodes-overcoming the barriers to global adoption," *Proceedings of the Institution of Civil Engineers-Civil Engineering*, vol. 168, no. 4, pp. 179–184, 2015.

[22] Y. Guo, G. Gong, C. Chin, and C. Zhang, "Structural design of concrete to EC2 and GB50010-2010: a comparison," *MATEC Web of Conferences*, vol. 175, p. 01039, 2018.

[23] China Ministry of Construction, *JGJ3-2010: Technical Specification for Concrete Structures of Tall Building*, China Architecture and Building Press, China Ministry of Construction, Beijing, China, 2010, in Chinese.

[24] M. Li, X. Lu, X. Lu, and L. Ye, "A preliminary comparison of the seismic design of tall RC frame-core tube structures between China and the United States," in *Proceedings of the 2013 World Congress on Advances in Structural Engineering and Mechanics (ASEM13)*, Jeju, Korea, September 2013.

[25] X. Lu, M. Li, H. Guan, X. Lu, and L. Ye, "A comparative case study on seismic design of tall RC frame-core-tube structures in China and USA," *The Structural Design of Tall and Special Buildings*, vol. 24, no. 9, pp. 687–702, 2015.

[26] H. Duan and M. B. D. Hueste, "Seismic performance of a reinforced concrete frame building in China," *Engineering Structures*, vol. 41, pp. 77–89, 2012.

[27] H. G. Kabtamu, G. Peng, and D. Chen, "Dynamic analysis of soil structure interaction effect on multi story RC frame," *Open Journal of Civil Engineering*, vol. 8, no. 4, pp. 426–446, 2018.

[28] Y. Li, X. Wu, W. Feng, and S. Bai, "Comparison between seismic performances of RC frames designed according to Chinese and European Codes (in Chinese)," *Journal of Earthquake Engineering Vibration*, vol. 27, 2007.

[29] China Ministry of Construction, *GB50011-2001: China Code for Seismic Design of Buildings*, China Architecture and Building Press, China Ministry of Construction, Beijing, China, 2001.

[30] H. Krawinkler and G. D. P. K. Seneviratna, "Pros and cons of a pushover analysis of seismic performance evaluation," *Engineering Structures*, vol. 20, no. 4–6, pp. 452–464, 1998.

[31] A. M. Mwafy and A. S. Elnashai, "Static pushover versus dynamic collapse analysis of RC buildings," *Engineering Structures*, vol. 23, no. 5, pp. 407–424, 2001.

[32] China Ministry of Construction, GB50010-2010: China Code for Concrete Design of structures, China Architecture and Building Press, China Ministry of Construction, Beijing, China, 2010.

[33] Ethiopia Ministry of Construction, *ES2-2015: Ethiopian Standard 2 Based on European Norm; Design of Concrete Structures: Part 1-1: General Rules and Rules for buildings*, Ethiopia Ministry of Construction, Addis Ababa, Ethiopia, 2015.

[34] L. Liu, *Concrete Structural Fundamentals Based on Chinese Concrete Design Standard GB50010-2001*, Wuhan University Technology Press, Hubei, China, 2004, http://www.techbook.com.cn.

[35] Ethiopia Ministry of Construction, *ES1-2015: Ethiopian Standard 1 Based on European Norms: Actions on Structures-Part 1-1: General Actions-Densities, Selfweight, Imposed Loads for Buildings*, Ethiopia Ministry of Construction, Addis Ababa, Ethiopia, 2015.

[36] China Ministry of Construction, *GB50009-2012: Load Code for the Design of Building Structures*, China Architecture and Building Press, China Ministry of Construction, Beijing, China, 2012.

[37] G. Shi, F. Hu, and Y. Shi, "Comparison of seismic design for steel moment frames in Europe, the United States, Japan and China," *Journal of Constructional Steel Research*, vol. 127, pp. 41–53, 2016.

[38] L. Kaihai and W. Yayong, "Researches about the conversion relationships among the parameters of ground motions in the seismic design codes of China, America and Europe," in *Proceedings of the World Conference on Earthquake Engineering*, Lisbon, Portugal, September 2012.

[39] MIDAS IT Co Ltd, "Midas Gen2015," in *Integrated Analysis and Design System for General Structures*, MIDAS IT Co., Ltd., Seongnam-si, Gyeonggi-do, Korea, 2015.

[40] Computers and Structures CSI, *CSI Analysis Reference Manual for SAP2000*, Computers and Structures, Inc., Berkeley, CA, USA, 2011.

[41] Computers and Structures CSI, *Structural Analysis Program SAP2000 Advanced 14.0.0*, Computers and Structures, Inc., Berkeley, CA, USA, 2009.

[42] M. Inel and H. B. Ozmen, "Effects of plastic hinge properties in nonlinear analysis of reinforced concrete buildings," *Engineering Structures*, vol. 28, no. 11, pp. 1494–1502, 2006.

[43] P. Naik and S. Annigeri, "Performance evaluation of 9 storey RC building located in North Goa," *Procedia Engineering*, vol. 173, pp. 1841–1846, 2017.

[44] C. B. Chadwell and R. A. Imbsen, "XTRACT: a tool for axial force-ultimate curvature interactions," in *Proceedings of the 2004 Structures Congress*, Nashville, TN, USA, May 2004.

[45] J. B. Mander, M. J. N. Priestley, and R. Park, "Theoretical stress-strain model for confined concrete," *Journal of Structural Engineering*, vol. 114, no. 8, pp. 1804–1826, 1988.

[46] A. Eslami and H. R. Ronagh, "Effect of elaborate plastic hinge definition on the pushover analysis of reinforced concrete buildings," *The Structural Design of Tall and Special Buildings*, vol. 23, no. 4, pp. 254–271, 2014.

[47] P. Tom and M. J. Nigel Priestley, *Seismic Design of Reinforced Concrete and Masonary Buildings*, John Wiley and Sons, Inc., Hoboken, NJ, USA, 1992.

[48] H. B. Kaushik, D. C. Rai, and S. K. Jain, "Effectiveness of some strengthening options for masonry-infilled RC frames with open first story," *Journal of Structural Engineering*, vol. 135, no. 8, pp. 925–937, 2009.

[49] M. S. Alhaddad, K. M. Wazira, Y. A. Al-Salloum, and H. Abbas, "Ductility damage indices based on seismic performance of RC frames," *Soil Dynamics and Earthquake Engineering*, vol. 77, pp. 226–237, 2015.

[50] W. K. Tso and A. S. Moghadam, "Pushover procedure for seismic analysis of buildings," *Progress in Structural Engineering and Materials*, vol. 1, no. 3, pp. 337–344, 1998.

[51] M. Causevic and S. Mitrovic, "Comparison between nonlinear dynamic and static seismic analysis of structures according to European and US provisions," *Bulletin of Earthquake Engineering*, vol. 9, no. 2, pp. 467–489, 2011.

[52] P. P. Diotallevi and L. Landi, "On the pushover analysis as a method for evaluating the seismic response of RC buildings," in *Earthquake Resistant Engineering Structures V 203*, C. A. Brebbia, Ed., p. 15, WIT Press, Chilworth, UK, 2005, https://www.witpress.com/elibrary/wit-transactions-on-the-built-environment/81/15058.

[53] PEER, Pacific earthquake engineering research center: strong ground motion database, http://peer.berkeley.edu/research/motions/.

[54] Seismosoft, SeismoMatch 2016: A Computer Program for Spectrum Matching of Earthquake Records, 2016, http://www.seismosoft.com.

[55] SeismoSoft, SeismoArtif 2016: A Computer Program that Generate Artificial Earthquake Accelerograms Matched to a

Specific Target Response Spectrum, 2016, http://www.seismosoft.com.

[56] American Society of Civil Engineers, *ASCE/SEI 41-13-Seismic Evaluation and Retrofit of Existing Buildings*, American Society of Civil Engineers, Reston, VR, USA, 2013.

[57] D. Vamvatsikos and C. Allin Cornell, "Incremental dynamic analysis," *Earthquake Engineering & Structural Dynamics*, vol. 31, no. 3, pp. 491–514, 2002.

[58] S. Cornell and R. Pinho, "Advantages and limitations of adaptive and non-adaptive force-based pushover procedures," *Journal of Earthquake Engineering*, vol. 8, no. 4, pp. 497–522, 2004.

[59] J. J. Bommer and A. S. Elnashai, "Displacement spectra for seismic design," *Journal of Earthquake Engineering*, vol. 3, no. 1, pp. 1–32, 1999.

[60] S. Akkar and J. J. Bommer, "Prediction of elastic displacement response spectra in Europe and the Middle East," *Earthquake Engineering & Structural Dynamics*, vol. 36, no. 10, pp. 1275–1301, 2007.